Automation Of A Solar Panel Test-Rig

Treviño Quintillà, Marc

Zubieta Mor, Ion

Bachelor's thesis in Electronic and Automatic Industrial Engineering

Degree Programme in Energy Technology

Vaasa, 2020

Acknowledgements

We would like to thank all the people we have come across during this stage. First, to all the classmates with whom we have shared and built our college life. Also, to all the teachers who have tried to prepare the best possible for the professional world that we will face by teaching us everything that was within their reach.

We would like to make a special mention to our tutor Philip Hollins to guide us throughout this project.

To Hans Lindén for providing us with all the necessary material and theoretical knowledge of the ModBus Protocol to be able to carry out this project as well as being a person who has found solutions to our problems throughout the process.

Finally, we would like to thank both the University of Lleida and NOVIA University for making this exchange possible and especially Roger Mäntylä for always being there and helping us throughout the stay.

Abstract

BACHELOR'S THESIS
Authors: Treviño Quintillà, Marc; Zubieta Mor, Ion
Degree Programme: Electronic and Automatic Industrial Engineering
Specialization: Energy Technology
Supervisor: Philip Hollins
Title: Automation Of A Solar Panel Test-Rig

Date: 14th August 2020 Number of pages: 81 Appendices: 2

The aim of this thesis is to construct a research tool for automatized tests on photovoltaic panels. The purpose is to create an instrument which enables the comparison of different types of solar panels in a controlled environment.

A program has been developed within LabVIEW and utilizing the ModBus Protocol is capable of controlling different parameters such as panel light intensity, applied load and energy meter data acquisition. A range of simulations has been performed for three different panels under the same conditions in order to be able to make some conclusions about which panel is better depending on each situation. It has been noticed that there is no significant difference in the output obtained by single-phase and thin-film 30W boards with the premise that single-phase is theoretically more efficient than thin-film.

Furthermore, the test-rig has also been used to study the behaviour of solar panels facing different shadow scenarios. Depending on the position of the shadow, the impact on the output power for the same solar panel can be from -1% to -99%. Finally, further research and different testing scenarios are suggested such as modifying the type of lights or analyzing the temperature of the panel and how this affects its efficiency.

Going further, this tool could be interesting and useful for a future study with different scenarios in order to understand better the behaviour of solar panels.

Language: English
Keywords: Solar test-rig, Photovoltaic, ModBus, LabVIEW

Table of contents

List of figures

List of tables

1. Introduction

One of the most serious problems the world is facing nowadays is the deterioration of the atmosphere and, consequently, climate change. Historical and current energy systems are dominated by fossil fuels (coal, oil and gas) which produce carbon dioxide (CO_2) and other greenhouse gases; the fundamental drivers of global climate change (Ritchie and Roser, 2018).

The last generation has been and is still in dire straits to accomplish a change in the way energy is being generated. As is well known, fossil fuels have an expiry date, which is getting closer and closer, so humans have the task of changing the way energy has traditionally been generated.

There are several options available nowadays in the field of renewable energies, such as wind, hydraulic or tidal energy. Among all the options, solar energy will take an important role to get to that target, as it gives a wonderful opportunity to generate magnificent amounts of energy in a sustainable way.

Solar power is one of the most environmentally-friendly energy sources. Overall, all Solar Photovoltaic (PV) technologies generate far less life-cycle air emissions per GWh than conventional fossil-fuel-based electricity generation technologies (Fthenakis, et al., 2008). Moreover, in (End-of-life management Solar Photovoltaic Panels, 2016) it is mentioned that over 90% of the materials in current solar panels can be recycled into the next generation.

An important advantage of solar PV is that it utilizes the most abundant renewable energy resource on the planet, the sun. Estimates show that there is 10,000x more solar energy coming to the Earth's surface than global annual fossil fuel demand (Student Energy, 2020).

With this thesis, it is intended to go deeper into this field and to create a tool that can be used to investigate and analyze the different types of solar panels, in order to get the most out of the greatest source of energy, the sun.

1.1. Aims and objectives

The aim of this study is to complement and improve a solar panels comparison carried out last year at Technobotnia Laboratory. The purpose behind it is to build a tool that allows the comparison of the different types of solar panels available in the market in different situations and simultaneously gain experience at renewable energy's field.

During the thesis' development Modbus Protocol based devices implemented through a LabVIEW interface will be used, comment on the importance of these communication technologies and demonstrate how they can be relatively easily implemented. This will also fulfil the aim of enlarging our knowledge and getting practical experience.

In order to meet this aim, the following objectives have been established:

- To assemble and use a solar panels comparison system utilizing a LabVIEW interface interconnected via Modbus for real-time monitoring and communication.
- To automate the variable resistor using relays. To streamline reducing the number of Modbus devices used to just one.
- To upgrade the methodology handled during shades such as preparing different PV shading scenarios.
- To enhance the storage and data output via LabVIEW with result presentation in Excel.

2. Solar photovoltaic

Solar photovoltaic (PV) is a technology that converts solar radiation into DC electricity using photovoltaic cells (Student Energy, 2020). Light shining onto a PV cell produces a voltage and a current to generate electric power through the use of semiconductors. A brief explanation of the operation will be made in the next section to understand better the operation of the different panels.

2.1. Operation of solar panels

There are several types of solar cells but the most common in usage and the marketplace are those whose composition is based on silicon. Although other kinds of solar cells are being developed with other compositions and other semiconductors, this thesis will be focused on the silicon-based PV panels.

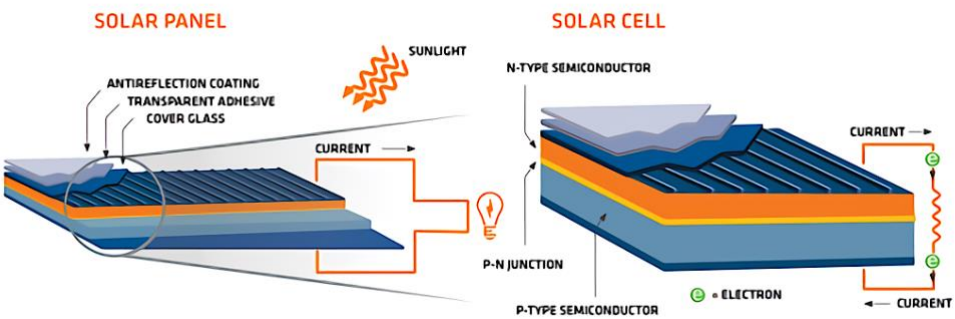

Figure 1: Solar cell layers representation (How Do Solar Panels Work?, 2016)

The most important parts of a solar cell are the semiconductor layers. Initially, electrons of the silicon base are not able to move to produce electricity. Atoms of phosphorus are injected in the upper layer of the cell producing what is known as “n” doping, and boron atoms are

injected in the lower one, originating a “p” layer. This modification of the semiconductor layers produces an excess of electrons in the n layer, which will make them move across the junction filling the gaps that boron produced. An area with non-electrons or holes influence known as the depletion region is formed, creating an electric field between p-n layers. When sunlight energy penetrates the n layer and interacts with this junction area, it forms new electron-hole pairs increasing the concentration of those in the corresponding layers and generating a voltage differential in the cell. As soon as a charge is connected between the p-n regions, electrons will begin to flow through it continuously supplying direct current. Because the amount of power produced by a single solar cell is relatively small, one to two watts, designers’ group solar cells together to form modules (better known as panels) that supply a more useful level of voltage, current, and power.

2.2. Types of solar panels

The technology of photovoltaic panels has been in continuous development for many years, which has led to currently enjoy a wide range of options for different types of solar panels. The different types of solar panels will be explained in the chronological order in which appeared. An overview of the three generations of the PV panels can be seen in Figure 2.

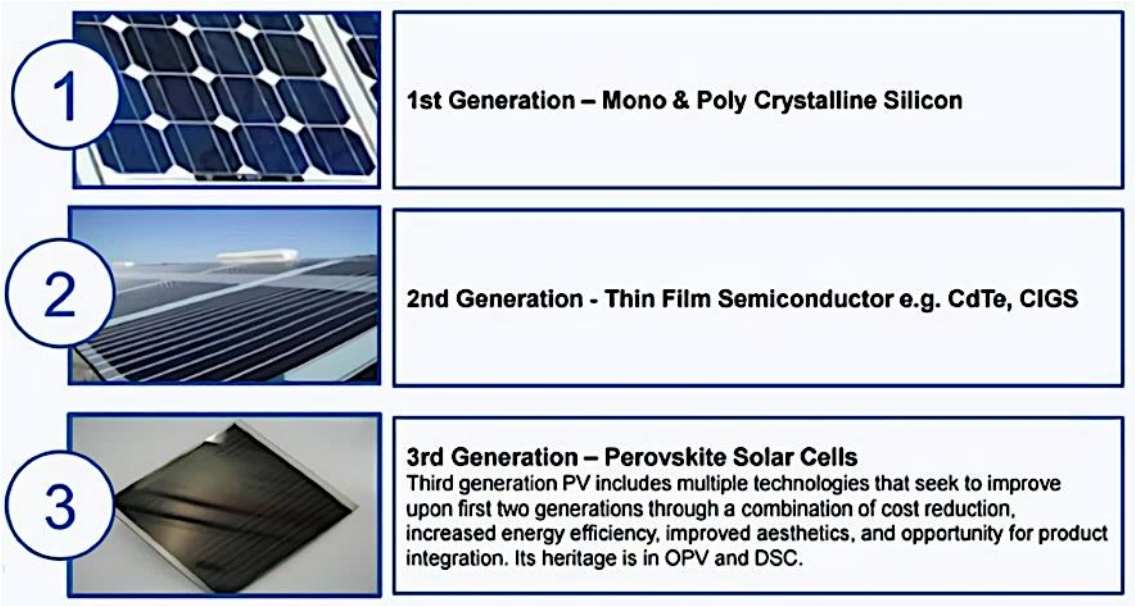

Figure 2: Generations of PV panels (Could DYE Transform into a “Mini-Tesla” of Solar?, 2016)

- First-generation PV panels:

These are the traditional types of solar cells, which are made from monocrystalline or polycrystalline silicon, are currently the most efficient solar cells available for residential use.

  - Monocrystalline Solar Panels (Mono-Si)

This is the oldest and most developed technologies. Monocrystalline panels are created from a single continuous crystal structure. They are characteristic of a dark colour and round shaped solar cells corners. (GreenMatch, 2020).

- Polycrystalline Solar Panels (Poly-Si)

It is the cheaper silicon panel type to produce, as they are made from multiple crystals rather than from a single crystal, but also for this reason they are less efficient than the monocrystalline. They have a rectangular shape and bluish tone due to their silicon derivates mixture. (GreenMatch, 2020).

- Second-generation PV panels:

Also called thin-film solar cells because when compared to crystalline silicon-based cells they are made from layers of semiconductor materials only a few micrometres thick. The combination of using less material and lower-cost manufacturing processes allow the manufacturers of solar panels made from this type of technology to produce and sell panels at a much lower cost. This type of solar cells is mainly used for photovoltaic power stations, integrated into buildings or smaller solar systems.

- Thin-Film Solar Cells (TFSC)

They are created by depositing a photovoltaic material onto a substrate, it is also a less expensive option. There are different types depending on the materials used in the process (amorphous silicon, copper indium gallium selenide, cadmium telluride, etc). We will focus on the "A-Si" ones, as we will also use this on the experimental part. (SURFACE Syracuse University, 2020).

- Amorphous Silicon Solar Cell (A-Si)

This type of solar panel uses a triple-layered technology, which is the best of the thin film variety. The efficiency of amorphous silicon solar cells has a theoretical limit of about 15% and realized efficiencies are now up around 6 or 7%, so they are cheap to produce but they have low efficiency. (SURFACE Syracuse University, 2020).

- Third-generation PV panels:

This new generation of solar cells is being made from a variety of new materials besides silicon, including nanotubes, silicon wires, solar inks using conventional printing press technologies, organic dyes, and conductive plastics. The goal is to improve on the solar cells already commercially available. Some of this "close to market" solar cells are:

- Biohybrid Solar Cell
- Cadmium Telluride Solar Cell (CdTe)
- Concentrated PV Cell (CVP and HCVP)
- Organic solar cells (OSC)
- Copper zinc tin sulphide (CZTS)

These new types of solar panels are still being developed or improved in order to be marketed on a large scale. All of them are good options like for example, bio-hybrid solar cells which are made by combining both organic and inorganic matter. The interesting thing about these cells is that the organic matter they use is "Photosystem I", a photoactive protein that recreates the natural process of photosynthesis. (SURFACE Syracuse University, 2020).

Another alluring kind of solar cell is the organic ones. In these cells, instead of using silicon as a semiconductor material, they are built using organic electronics and carbon-based materials. The peculiarity of these cells is that, apart from being able to be produced as printable, they are flexible which allows us to install them almost anywhere we want. (Ameri, T., Dennler, G., Lungenschmied, C. and Brabec, C. J., 2009).

Three panels (a pair of thin-film and one monocrystalline) will be used while doing the experiments. In Figure 3, it can be seen the percentage of the annual production of each of the most common types of PV panels. Currently, the most used are the polycrystalline ones (as Multi-Si in the legend).

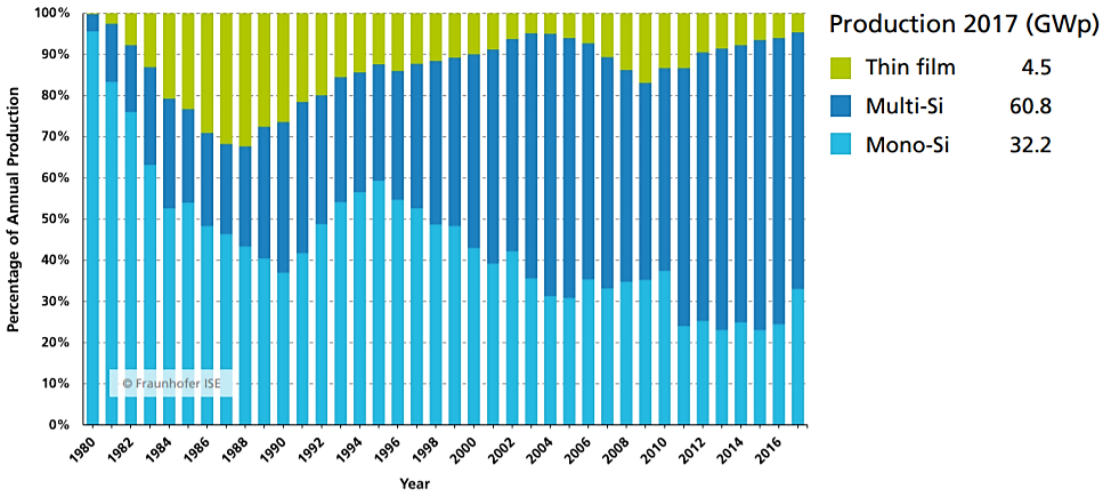

Figure 3: Percentage of global annual production (Anon., 2020)

To get an idea of the cost of solar panels according to their type, the average prices found on the market will be briefly explained below. In addition, in Figure 7 from section 2.4 a graph showing the decline in the price of PV panels from 1977 to the present day can be found.

Monocrystalline panels are the most expensive as they are also the most efficient. The average cost of these is 0.189$ per watt.

Polycrystalline panels used to be cheaper than the monocrystalline ones but nowadays the price is similar. These panels can be found at an average price of 0.187$ per watt.

The thin-film panels are the newest technology compared to the two previous types, therefore the price of these has not yet dropped that much. The average price of these panels is 0.213$ per watt.

It should be noted that the prices provided are the average price of PV panels that can be found in the United States as of 20th May 2020. These prices are updated weekly and tax excluded. (PVinsights, 2020).

2.3. World usage of solar energy

According to the global study conducted by the "BP" corporation (Anon., 2019), the world's cumulative installed solar power in 2018 was 487.829 MW. Compared to 2017 data, when the cumulative was 392.263 MW, it represents an increase of 24.4% in just one year. The leading country on this renewable energy is, by a large majority, China. Their generation capacity represents 36% (175032 MW) of the world's generation capacity. In Figure 4, the main producing countries can be seen.

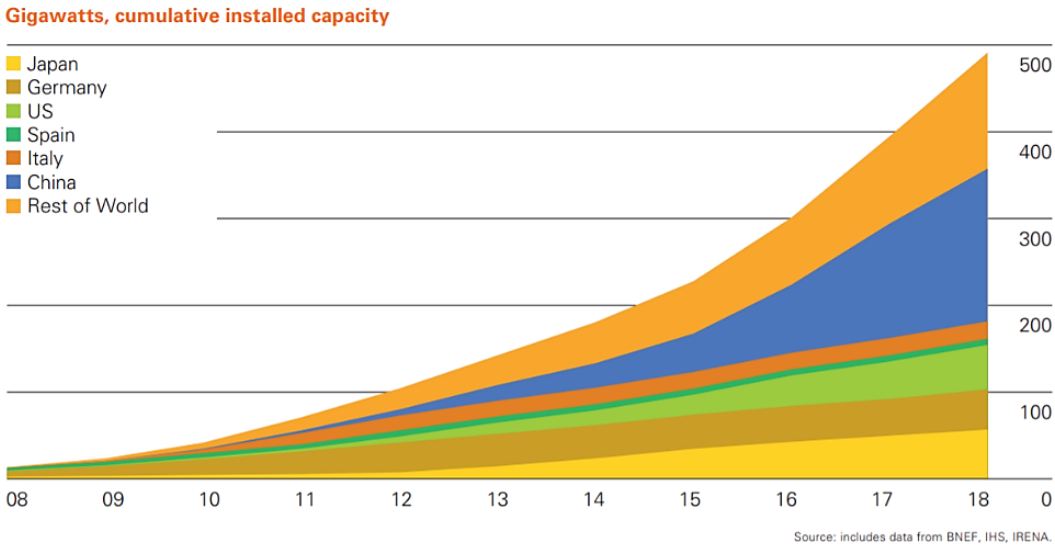

Figure 4: Global solar PV generation capacity (Anon., 2019)

Focusing on the data concerning Finland in Figure 5, it can be seen that in this country it is not much common the usage of this kind of renewable energy. The cumulative installed capacity is just 125 MW, which compared to other countries is fairly low capacity. For example, in Spain, there is a capacity of 7048 MW but it must be borne in mind that it is a sunny territory. (Anon., 2019).

Compared to its neighbouring countries of Scandinavia, it can be concluded that Finland was not focusing its efforts on developing their solar energy during the past years, at least not as much as Denmark, which from 2011 has been improving their capacity at a very high rate, as can be seen in Figure 5.

Despite these facts, during 2018, the installed solar energy capacity of Finland grew up 68.5% which is the second-largest growth in Europe, behind Hungary who increased their capacity by 93.3%. (Anon., 2019).

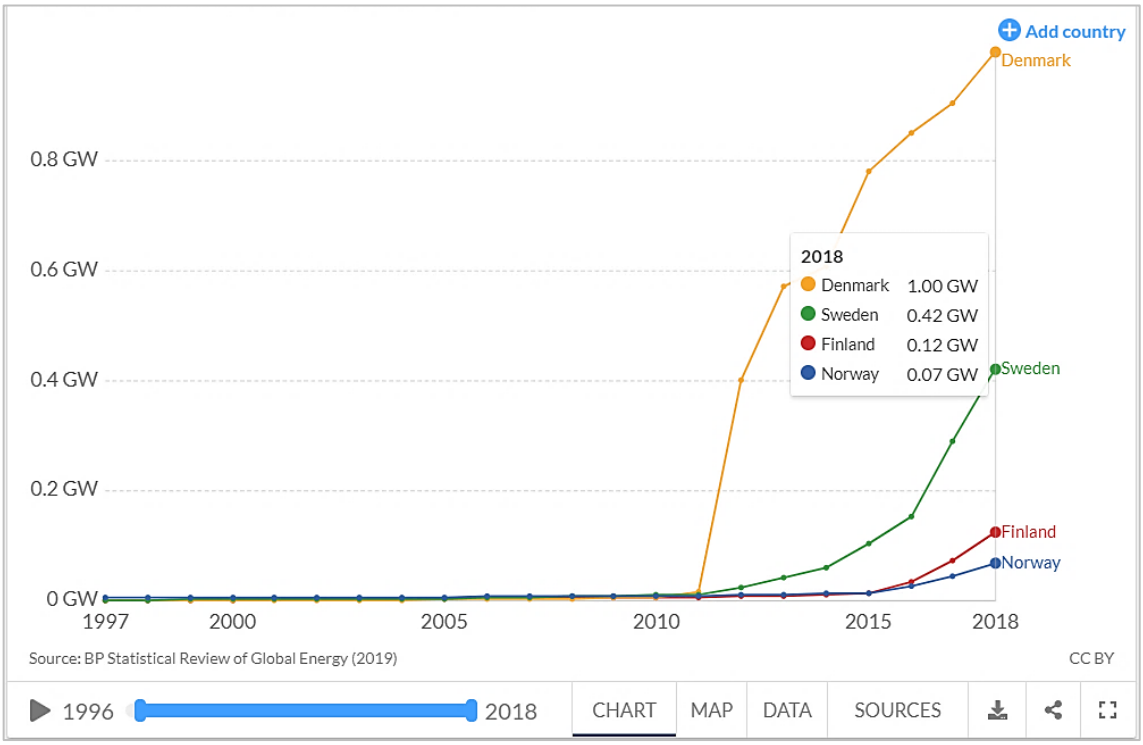

Figure 5: Installed solar energy capacity, 1997 to 2018 (Solar energy generation, 2019)

Please note that the data analysed in this section refers to 2018. The study was published in mid-2019 with the data from the previous year. It is the most recent reliable study available, as the 2019 study has not been published yet.

2.4. Analysis and forecasts from 2019 to 2024

During 2018 the total of new installations globally was 96 GW, a similar growth that in 2017. This increase represents 29% of more solar power generation, but despite this rapid growth, solar energy just represents 2.2% of global power generation. (Anon., 2019).

China took advantage of solar PV power generating capacity with 44 GW of new installations, which represents almost half of the total growth in global solar capacity. The following regions in terms of growth were India, the US and the EU with around 8 GW each. (Anon., 2019).

The predictions indicate that the greatest growth will be experienced in distributed photovoltaic panels, due to improvements in policies and lowering on the costs, which will lead to a total distributed PV capacity more than double of nowadays by 2024. However, with this increment, just 6% of the global technical potential will be used. This data can bee seen reflected in Figure 6.

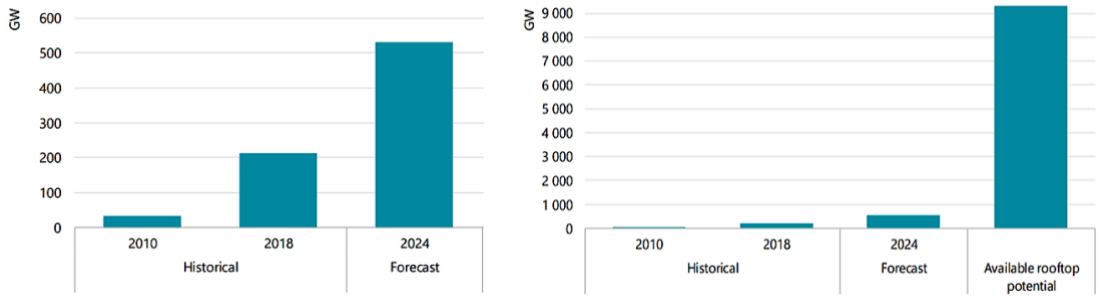

Figure 6: Distributed PV total installed capacity (Anon., 2020)

The expected increase in solar energy use can be justified by the following 5 factors:

1. Climate change agreement in Paris:

A significant contributing factor to the solar industry increase was the climate change agreement in Paris, established in early December 2015 and agreed by Nice representatives from 195 countries. The aim of the agreement was to reduce carbon emissions worldwide and limiting global warming. (United Nations Climate Change, 2020).

2. Low-Cost equipment:

The declining cost of solar energy equipment is probably the leading reason for the solar industry's growth. Next, it can be seen a graph showing this decrease in the price of silicon PV cells per watt. (IENE Institute of Energy for South-East Europe, 2020).

Since solar cells were first marketed, the price has been steadily decreasing until today, so those can be found at an affordable price. (IENE Institute of Energy for South-East Europe, 2020).

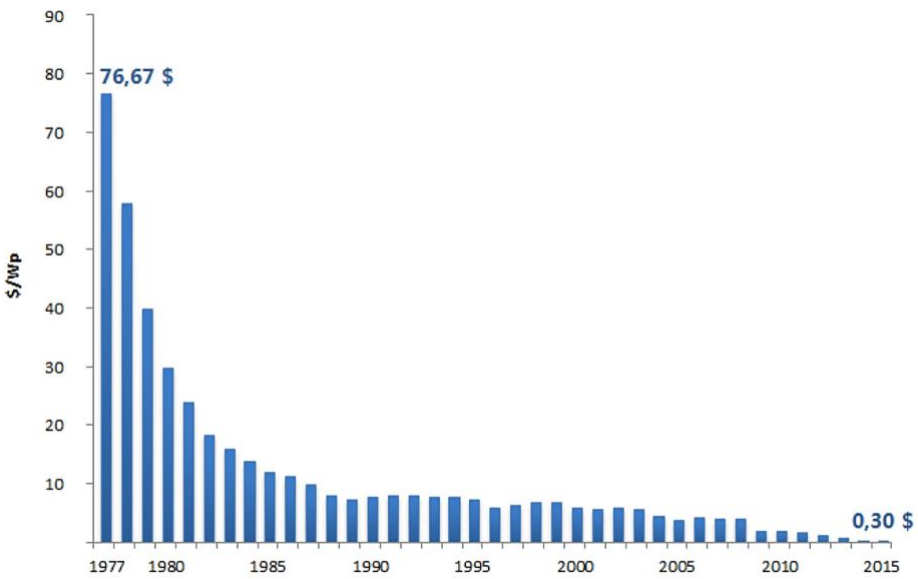

Figure 7: Price of crystalline silicon PV cells (in $/Wp) (Wikimedia Commons, 2013)

3. Policies and tax credits:

Governments around the world are giving some facilities to the customers through policies that encourage people to switch to renewable energy. Through this type of incentives, costs are further reduced when implementing a solar photovoltaic system. (Renewable Energy World, 2017).

4. Marketing and cultural demand:

The popularity of solar energy is in constant growth. Companies usually display their solar panels on their buildings so as to show people their interest, investment, and dedication to renewable energy. It is a method by which to exhibit their green credentials and try to attract more consumers. (WebFX Solar Marketing, 2020).

5. Battery storage:

A field in which many developments are also being made is batteries. Modern batteries essentially use saltwater as the only electrolytic, a much more environmentally friendly way compared to the old types that are loaded with sulphuric acid. The price of batteries, like those of solar panels, is in constant decline. (GreenMatch, 2020).

3. Methodology

The developed tool consists of four connected main parts. First of all, the relays board with which the resistances train will be short-circuited. Then, the energy meter which will read the measurements extracted from the solar panel with a certain resistance. After that, a control dimmer that will be connected to a light source that will simulate the sun that feeds the PV panel studied. Finally, the connections necessary to transport the energy generated by the PV panel to the rest of the circuit.

All these parts will be connected to the computer using the ModBus RTU Protocol, with which the energy meter, the control dimmer and the relay board must be compatible.

3.1. Materials and devices needed

All the materials mentioned in the following list have been provided by NOVIA University, specifically, equipment from the Technobotnia's laboratory. The full equipment setup can be seen in Figure 8 with full documentation found in Appendix 1.

Figure 8: Setup overview (Authors' own, 2020)

The materials and devices used to carry out this project are listed below:

- The panels wanted to be compared. In that case, a monocrystalline and two amorphous will be compared.

- A halogen floodlight that will simulate the sunlight. Note that to make that study as most realistic as possible, a powerful lamp will be needed due to simulating a sunny day means reproducing 120 Klux.

- A control dimmer compatible with ModBus RTU Protocol to adjust the wanted output of the halogen lamp. On that account, a DMX dimmer will be used with a DMX to ModBus converter, concretely, DMX-512 from RESI.

- A relays board compatible with ModBus RTU Protocol considering that as more relays, more load combinations can be made. In that event, an 8 relay channel board model R421A08 will be used.

- Different resistors which available the connection of them to the relays board and which combined can fulfil the load expectations and the size wanted to take for each iteration. The idea is to have 8 different selectable resistances which are 0.5Ω, 1Ω, 2Ω, 4Ω, 8Ω, 16Ω, 32Ω and 64Ω but those resistors were not available. Under these circumstances, the following resistances were used to obtain the desired load. The

resistors used are 1 of 0.5Ω, 1 of 1Ω, 1 of 2Ω, 1 of 4Ω, 4 of 8Ω, 1 of 10Ω, 1 of 22Ω and 1 of 56Ω.

- An energy meter compatible with ModBus RTU Protocol capable of measuring voltage, current and power. Acu DC 243 has been chosen to be used for this occasion.

- Two power suppliers. Any type of supplier is valid, but the used for this project is model 72-2540 from Tenma.

- A computer with the LabVIEW program and Microsoft Excel installed.

- An RS485 to USB module to connect the devices to the computer.

- Wires with different colours and lever nuts to make easier and more organized connections.

3.2. Modbus Protocol configuration

This project has been carried out with just one ModBus interface to the computer, which was one of the objectives. A requirement for this to be possible is that all slaves must be configured with the same parameters and have a different ID for each.

All of these parameters are predefined by the manufacturer and is needed to check if all the devices are compatible and if these parameters can be modified by the user. You have to check the datasheets and user's manuals of the devices to know how to modify the parameters if possible and if not, which are the defined parameters of the device.

For that project, the following parameters were chosen:

Baud rate = 9600 Data bits = 8 Stop bits = 1 Parity = None

After setting all the devices parameters, it is recommendable to test if the device is responding with the parameters set. To do that, QModMaster can be used.

3.3. ModBus Protocol configuration: control dimer

To set correctly the adequated parameters to the control dimer, both the converter and the DMX will be adjusted. As can be seen in Figure 9, the DMX to RS485 converter has a DIP-switch module. Following the DMX-512's datasheet, the first two DIP-switches (named BR) should be to the OFF position in order the converter works with a baud rate of 9600Bd. The next DIP switch (named IF) should be to the ON position so RS485 interface it is being used. The last DIP switch (named FD) should be to the OFF position so it will be using the unit ID from the flash memory. Unit ID can be modified with RESI's Modbus Configurator software. This device will be working with unit ID = 1.

For the DMX, once connected to the power, you must click on the MENU button of the device until the letter A and three digits appear on the screen of the device. The number following the letter A will be the address + 1, adjustable with the other buttons on the device. You must take that into account because ModBus addresses start with number 0 meanwhile the control dimer starts with number 1.

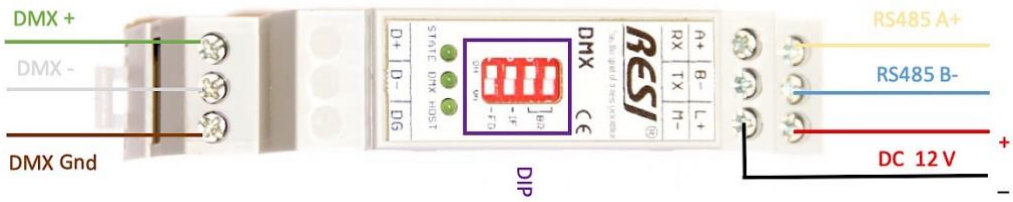

Figure 9: RS485 to DMX converter with DIP framed (RESI - Modified by authors, 2015)

3.4. ModBus Protocol configuration: relays board

About the relays board model R421A08 being used, unit ID is selected with the DIP-switches on the board. Unit ID will be set to 2. Figure 10 shows where DIP-switches are and, in that case, position 2 should be activated (to the right) and the rest deactivated (to the left). More information about the DIP-switches can be found in R421A08 datasheet.

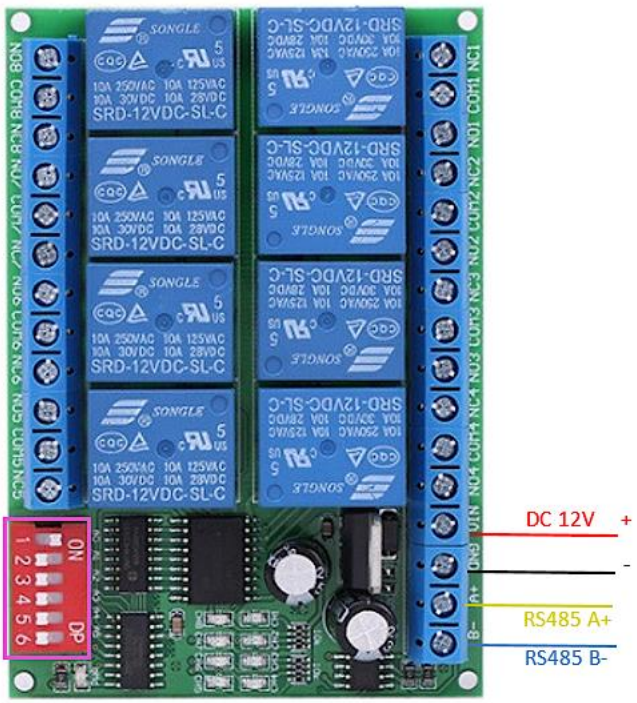

Figure 10: Relays board with DIP module framed (Anon. - Modified by authors, 2020)

3.5. ModBus Protocol configuration: energy meter

Referring to the power meter, the ModBus Protocol settings must also be configured. To enter the parameter setting mode, you must hold down the "F" and "V/A" buttons simultaneously when the device is turned on. Then, you will be required to type in a password on the "PASS" screen. Enter a password or leave it as default "0000" if it was not changed. Press the button "V/A" to enter the system parameter settings mode. Once inside the setting mode, the "F" button will change a setting or enter edit mode while the "V/A" button will confirm the changes or go to the next screen. When inside edit mode, button "F" can be used to increase the number of the flashing digit while "V/A" button can be used to switch the flashing digit and on the last digit to confirm the change, then the digit should stop flashing. For a more visual explanation, section 3.2 General Parameter Setup of the user's manual can be consulted.

Within the parameter setting mode, the communication address screen must be searched, with an "add" label. The energy meter unit ID has been set to 3. The next step should be to set the baud rate to 9600Bd. This can be done in the baud rate screen with a "bps" label. Finally, the parity can be selected in the parity screen, recognizable by the "chec" label that will be set to none, non1 in that case.

3.6. Assembly of the system

Next, the assembly process of the four steps mentioned above will be explained in detail. To facilitate the assembly process, explanatory images have also been added showing the connections to be made.

3.6.1. Step 1: Relays board

The first commission of that part would be to connect the relays board to the computer through the RS485 to the USB connector. To do that, it might be useful to look at Figure 11 where is shown how the connections are made.

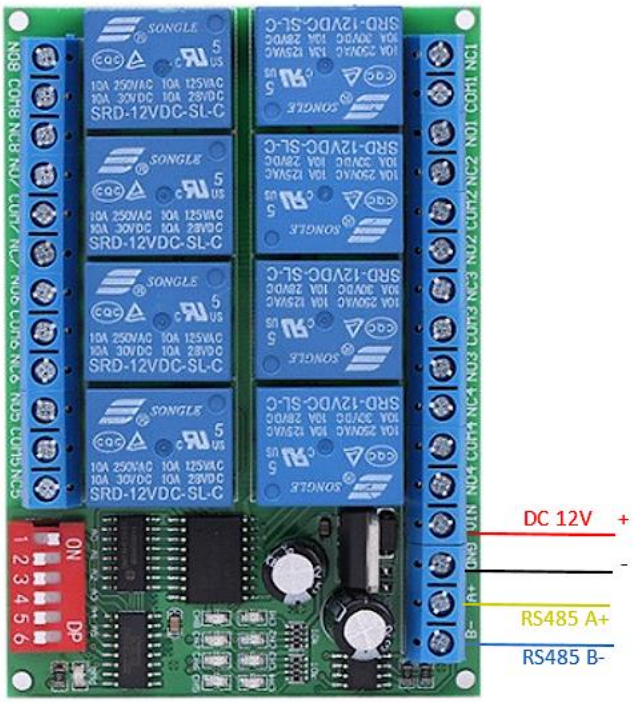

Figure 11: Relays board wiring diagram (Anon. - Modified by authors, 2020)

As pointed in Figure 11, you might have realized the board requires an input of 12V (voltage range 9V – 13V) which can not be offered by the USB to RS485 board due to it only offers 5V or 10V. Therefore, a voltage supplier will be used to fulfil the input voltage and only data pins will be connected to RS485. Voltage supplier will be set to 12V.

The last thing would be connecting the resistors train within the correct order. As it was designed to have a minimum step of 0.5Ω and a range from 0.5Ω to 127.5Ω, the order of the resistors will be the one shown in Figure 12.

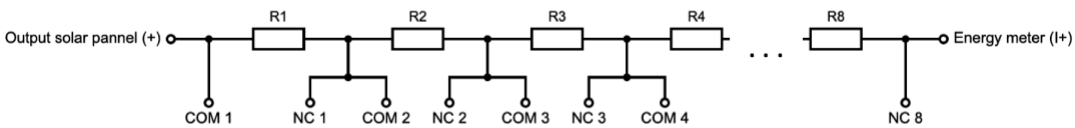

Figure 12: Resistior's train (Authors' own, 2020)

Starting from the left side of Figure 12, it can be seen that current will be fed by the solar power output which will be also feeding the pin COM 1. Then, the first resistor will be connected and later, before connecting the second in series, using a lever nut we will connect one cable to pin NC 1 and another to pin COM 2. From this point, the assembly will be repetitive as it can be seen in the figure. After connecting the last resistor, the output will be connected to pin NC 8 on the one hand and the I + input of the energy meter on the other. In this way, the wanted resistance can be selected by combining the opening of the relays.

3.6.2. Step 2: Energy meter

A similar procedure of the first step has to be carried out. First thing would be to connect the energy meter to the computer through the RS485 connector. To get an idea of how the connections have to be made, Figure 13 can be checked. As this project will be carried out with just one ModBus device, ModBus wires of the energy meter have to be connected to the same pinout where the relay board was connected on the previous step. Lever nuts can be used to have an organized and simpler connection.

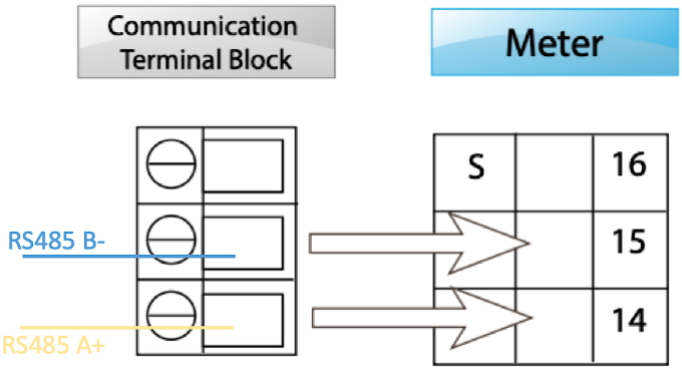

Figure 13: Wiring diagram RS485 to energy meter (User's manual energy meter AcuDC 240 Series - Modified by authors, 2018)

Once the energy meter is connected to the computer, it is time to get to the energy meter those data that wanted to read. Hence, voltage and current will have to be provided to the energy meter. To achieve this, Figure 14 will help make the connections correctly. It should be noted that the energy meter used allows several connection options to measure the same type of data (Accuenergy, 2018). The direct connection option has been chosen on this occasion.

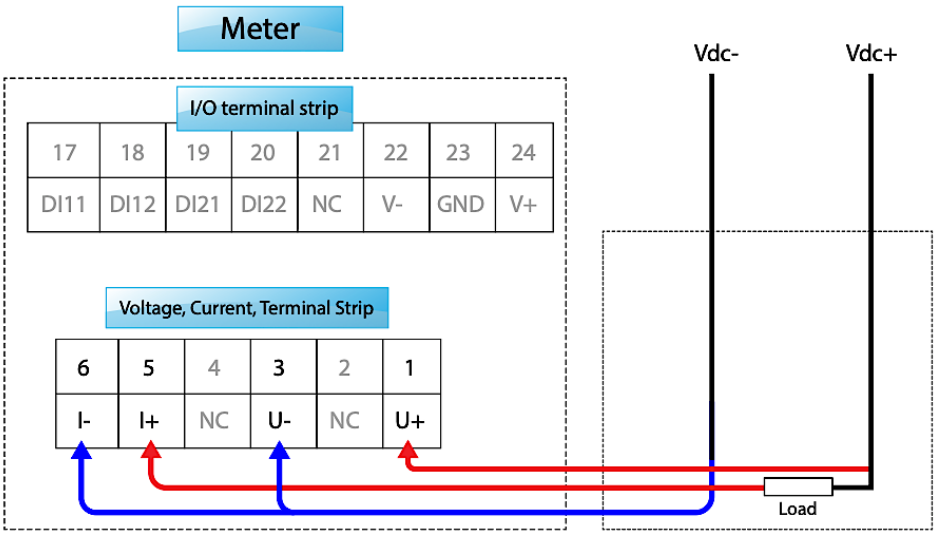

Figure 14: Wiring diagram direct connection energy meter (User's manual energy meter AcuDC 240 Series, 2018)

As it can be seen in Figure 14, to connection number 1 (U+), the positive wire from the solar panel output will be hooked up; to connection number 5 (I+), a wire from the output of the resistors train will be hooked up as commented before on the previous step; to connections 3 (U-) and 6 (I-), the negative wire from the solar panel output will be hooked up. User's manual can also be checked for a better understanding.

The energy meter also needs power supply as can be read in User's manual. The low voltage DC option will be chosen and another power supply will be needed because the energy meter needs to be fed up with at least 20Vdc. Wiring diagram of the power supply can be found in Figure 15.

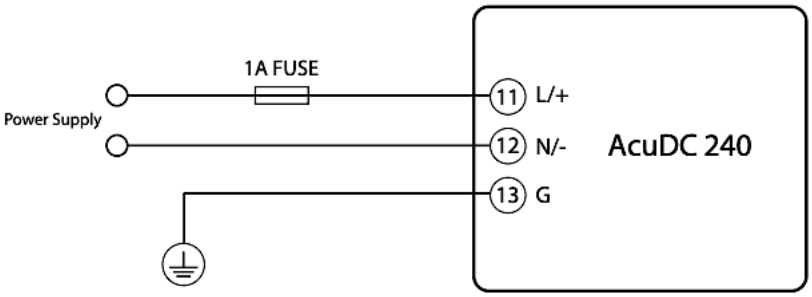

Figure 15: Wiring diagram power supply energy meter (User's manual energy meter AcuDC 240 Series, 2018)

3.6.3. Step 3: Floodlight and control dimmer

The same methodology will be adapted to the last part of the assembling. To connect the control dimmer (Stairville DS-2 RF DMX) to the RS485 bus, an adaptor will be needed. RESI-DMX-MODBUS will be used.

To connect the RESI-DMX-MODBUS converter to RS485, follow the wiring diagram that can be found in Figure 16.

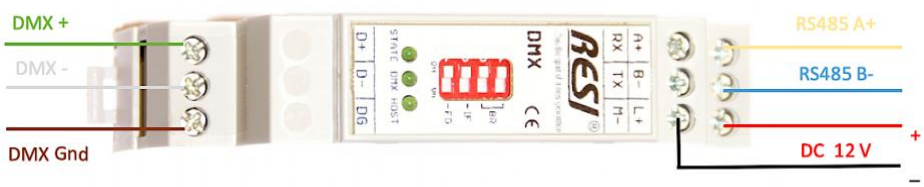

Figure 16: Wiring diagram of RESI-DMX-MODBUS converter (RESI - Modified by authors, 2015)

The RESI-DMX-MODBUS converter also needs a power supply. That device tolerates inputs from 12V to 48V which means that the power suppliers used for the previous devices can be used for both devices. In that case, the power supplier set to 12Vdc will be supplying both, the relays board and the DMX to ModBus converter.

Next would be to connect the DMX device. The control dimer employed uses a 3-pin wire input, concretely an XLR-3. Then, a 3 pin XLR male terminator must be used, in which the appropriate connections must be made, taking into account that pin 1 corresponds to the grounding, pin 2 to DMX - and pin 3 to DMX +. To make the link it is recommendable to use a 3 wires cable.

Figure 17: XLR-3 male terminator and connection diagram (Stairville DMX Terminator XLR 3-Pol, 2020) (XLR-3, 2020)

Once assembled, it would be time to connect the DMX to RS485 converter to the control dimer by plugging the 3-wire cable with the XLR terminator to the Stairville DS-2 RF DMX device.

As it can be seen by considering the device, the Stairville DS-2 RF DMX, this also needs to be connected to a 230V AC power outlet.

To complete this step, all that remains is to connect the floodlight by plugging it into the DMX.

3.6.4. Step 4: Solar panel

The last step in the assembly process is to connect the solar panel to the rest of the system so that we can analyse the performance of the panel.

The solar panels used for this project are very easy to connect, as they have an integrated adapter from which both polarities (positive and negative) come out. Regarding for the positive polarity cable, it must be connected to the energy meter (for voltage measurement) as well as to the first resistor and the COM 1 port of the relay board as explained in step 2.

Concerning for the negative polarity cable, it must be connected to the energy meter to both the negative polarity of the voltage and the current as also explained in step 2. Reminding that to get more organized and easier connections lever nuts can be used.

In Figure 18, it is shown how the connections to the panel can be made.

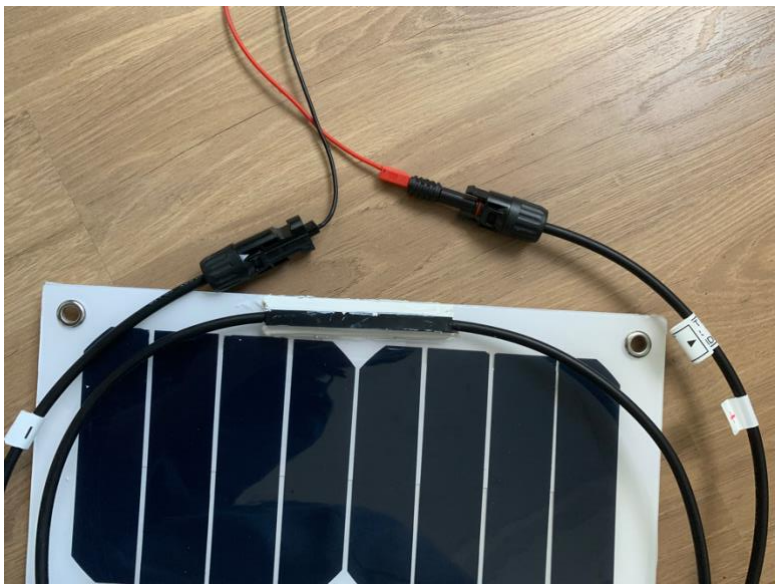

Figure 18: Connection to the solar panel (Authors' own, 2020)

It is important to note that the automatic testing system is designed to operate in an enclosed space, whether it is a laboratory, a classroom or a room of its own. If it was wanted to have the solar panel located outside, outdoors, it would be necessary to add a safety element to prevent the connection from being damaged due to weather conditions. An MC4 connection, designed for such conditions, should be used. It is worth noting that the wiring of the plate is doubly protected, as it consists of two layers of plastic that cover the copper just to be safer due to the exposure they have.

4. LabVIEW

In this section of the thesis, it will be explained as clearly as possible the program that has been created in LabVIEW and also how to make use of it.

4.1. Programming the LabVIEW interface

To start with the explanation of the program, the first thing would be to see an overview. In it, the different sections or blocks of which the program is made up are highlighted. In the image provided, the details cannot be clearly seen, as the aim of this is simply to give an overview. Later on, each section will be explained in detail.

The sections that can be seen in Figure 19, are marked with a red box and a letter. These are the sections corresponding to each letter:

- A – ModBus master
- B – Floodlight loops counter
- C – Floodlight power selector
- D – Resistors loops counter
- E – Relay board control
- F – Data format converter
- G – Data matrix generator
- H – MS Excel report generator

In the overview, the different loops and flat sequences blocks that have been used are also marked with arrows. The green arrows indicate the three flat sequences and the purple ones indicate the three loops that have been used.

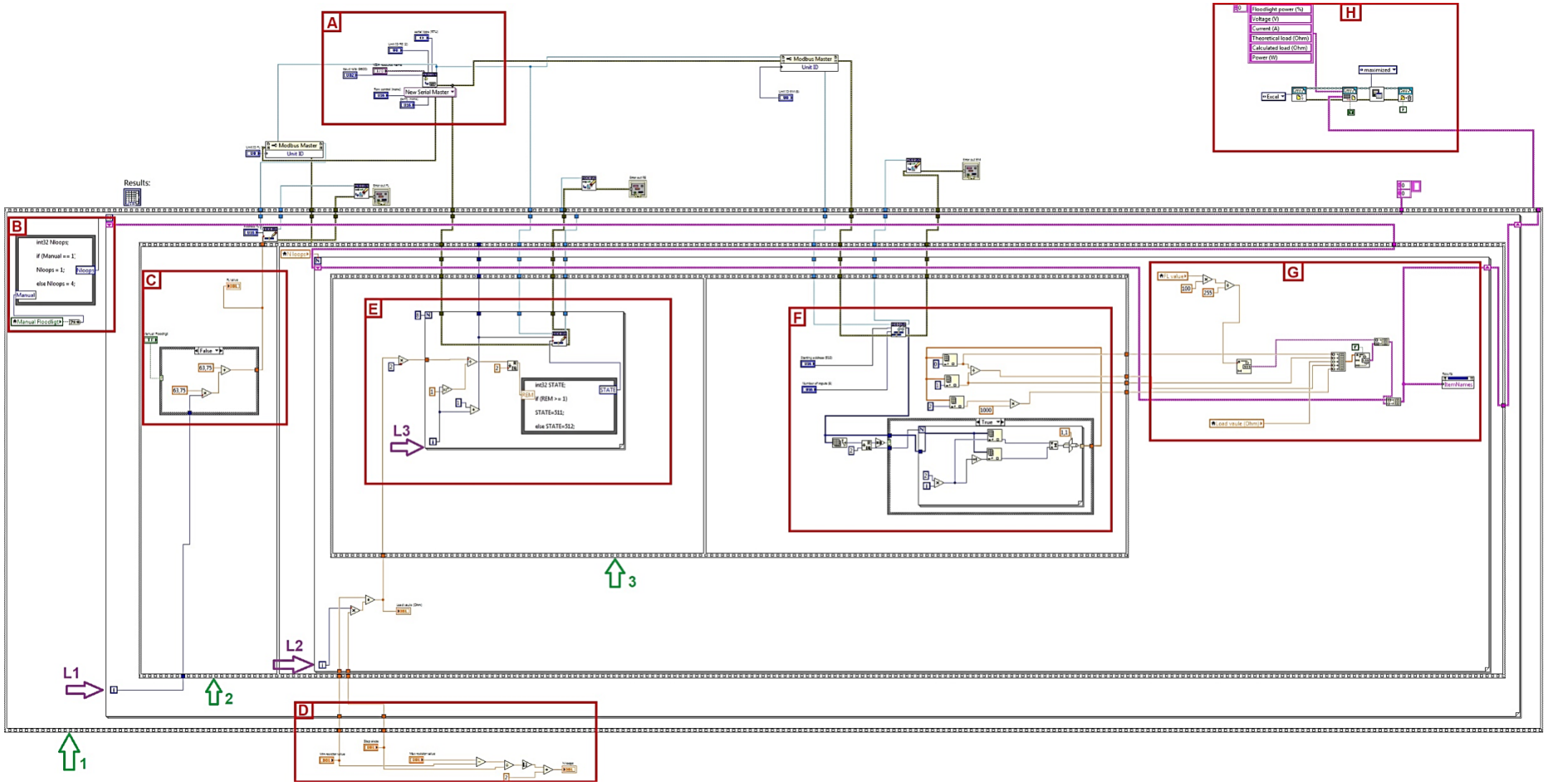

Figure 19: LabVIEW program general overview (Authors' own, 2020)

The program may seem confusing at first, but by analysing it in parts and in the corresponding order in which it is executed, it can be clearly understood. Before going into the details of each section, a brief explanation of the loops and flat sequences in the program will be made.

Generally speaking, it all starts in block A (red rectangle A), where the ModBus master is configured. Next, the D block (red rectangle D) is executed, which calculates the number of iterations of the L2 loop (purple arrow L2). Once this is done, the program enters in the first flat sequence (green arrow 1). This only serves as a general framework and prevents all data generated within it from being sent to the H block (red rectangle H) until it is fully executed.

Within the sequential 1 (green arrow 1), there is the loop L1 (purple arrow L1), which will be repeated once or four times, depending on the answer given by the block B (red rectangle B).

Within loop L1 (purple arrow L1) is the sequence block two (green arrow 2) which is divided into two parts. The characteristic of the flat sequences is that, until everything in the first block is executed, the next one is not started. That is until the C block (red rectangle C) has been completely executed, the L2 loop (purple arrow L2) will not start.

Within the L2 loop (purple arrow L2), in which the number of iterations must have been previously calculated by the D block (red rectangle D), there is the sequential 3 (green arrow 3) which will be executed first and then the G block (red rectangle G).

Within the flat sequence 3 (green arrow 3), comprised first by block E (red rectangle E) and then by block F (red rectangle F). Remember that block F (red rectangle F) will not run until the end of block E (red rectangle E) due to the flat sequence.

In the last step of the program, all the data that have been generated in flat sequence 1 (green arrow 1), is sent to the H block (red rectangle H) to be written in an MS Excel file.

Now that the general operation of the whole program has been explained, a detailed explanation of the mentioned blocks (red rectangles A to H) will be made.

4.1.1. Block A – ModBus master

In this program, only one USB to RS485 board is used, so only one ModBus master will be needed to control the three devices (floodlight, relay board, energy meter) which are the slaves.

In block A, the ModBus master is configured, all configuration parameters (serial type, unit ID, baud rate, flow control, parity) are entered by creating “controls” and also the connections to the three slaves are made from it.

As can be seen in Figure 20, from the ModBus master icon, apart from the configuration parameters mentioned, there is a light blue connection and a yellow/black connection.

These connections will be linked to the icons of the three slaves. The light blue colour to send the information and the yellow/black colour to transmit the possible errors that occur during the execution of the program.

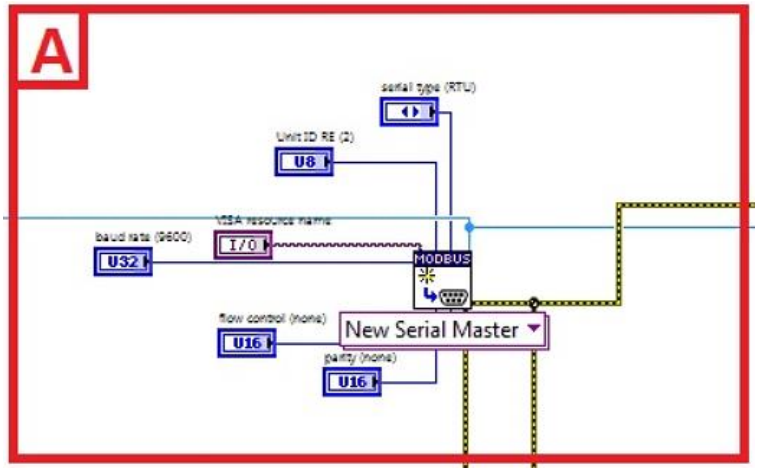

Figure 20: Detailed view of block A (Authors' own, 2020)

4.1.2. Block B - Floodlight loops counter

The user can choose whether to enter a fixed floodlight power value or whether to have the power automatically increased in four steps (25%, 50%, 75% and 100% of the power output of the floodlight).

If the user chooses the manual mode, the reference will have a boolean value of 1, while if the automatic mode is chosen this reference will have a value of 0.

By means of a code block that can be seen in Figure 21, the value of this reference is analysed. When the value is 0 (automatic) 4 iterations will be done in the L1 loop, while if the value is 1 (manual) only one iteration will be done in the loop.

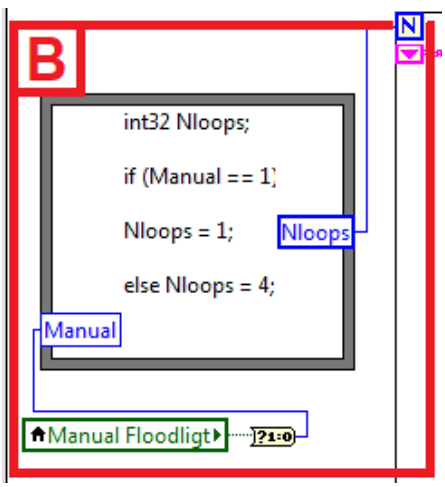

Figure 21: Detailed view of block B (Authors' own, 2020)

4.1.3. Block C - Floodlight power selector

In block C, the value of the floodlight power is set. As in the previous block, it will be analysed whether the user has chosen the automatic or the manual mode.

If the automatic mode has been selected, the case structure will have a false value and its code will be the one that can be seen in Figure 22. In case the manual mode has been selected, the case structure will have a true value and its code can be seen in Figure 23.

Bearing in mind that the value of the floodlight power is measured on a scale of 0-255, it can be concluded that every 25% of the power would equate to 63,75. That is to say,

63,75 = 25% of power output

127,5 = 50% of power output

191,25 = 75% of power output

255 = 100% of power output

Within the case structure when the automatic mode is activated, two operations are performed resulting in the reference value of the floodlight power (FL value). This reference will be used later in the G block. The value obtained from the case structure is also sent to the slave corresponding to the floodlight so that the power change is executed.

The blue wire that can be seen at the bottom of the image, which is multiplied by a fixed value of 63'75, is connected to the number that indicates in which iteration the L1 loop is located. The numbering of the iterations starts from zero, for this reason, an addition operation is needed after the multiplication.

In the first iteration of the L1 loop, the result of the initial multiplication would be 0, to which is added 63'75, obtaining a total result of 63'75 (25%) in the first iteration of the loop. With each new iteration, the floodlight power value increases by 25%, until it reaches 100%.

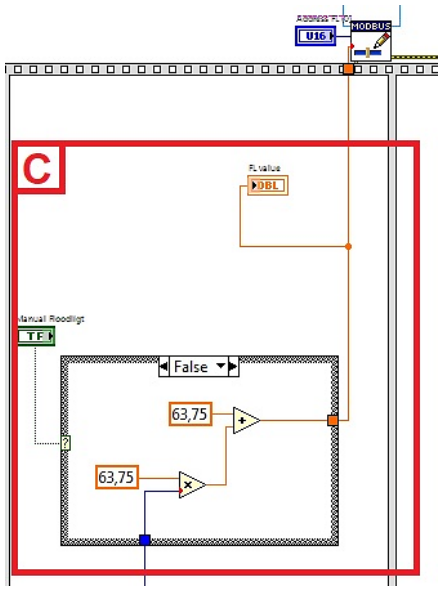

Figure 22: Detailed view of block C - Case structure = false (Authors' own, 2020)

The case structure for the manual mode is simpler, since it simply reads the value of the floodlight power that has been entered by the user, and is saved in the reference "FL value" to be used later.

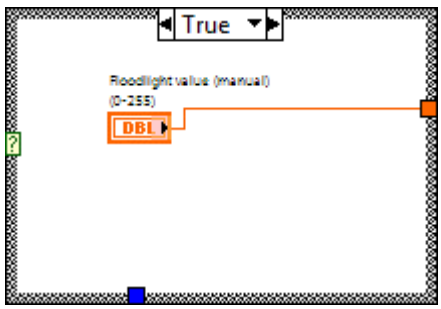

Figure 23: Detailed view of block C - Case structure = true (Authors' own, 2020)

4.1.4. Block D - Resistors loops counter

In the D block, the number of iterations that the L2 loop must give is calculated from the user entered values of "Min resistor value", "Max resistor value" and "Step size". The number of iterations that the L2 loop must-have is adjusted to the user's desire, allowing to select the corresponding load during the whole test.

The operations that are carried out in this block are given by the following equation.

$$Nº\ loops = \frac{Max_{\ resistor\ value} - Min_{\ resistor\ value}}{Step\ size} + 2$$

Note that a two is added to the division result because the iteration numbering starts at 0 and the first value must be discarded after each floodlight power change because the value shown is not real.

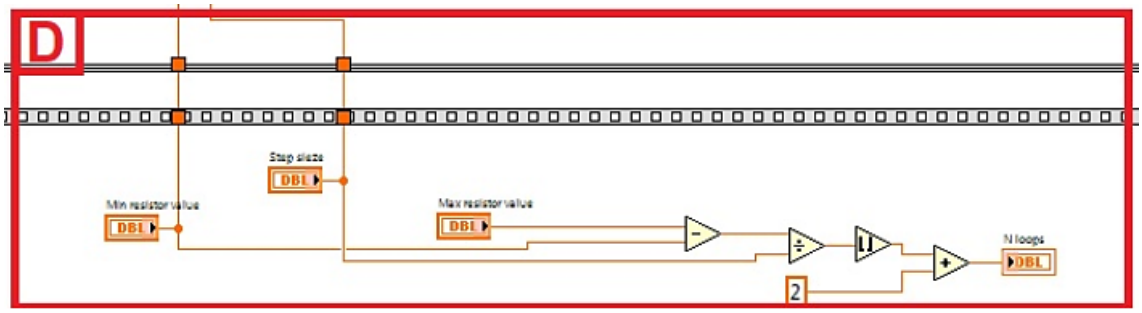

Figure 24: Detailed view of block D (Authors' own, 2020)

4.1.5. Block E - Relay board control

Within the E block is the L3 loop. This loop is operated with a fixed value of iterations, which are 8 since the relay board consists of eight switches that will be opened and closed to achieve the combinations of resistors that allow selecting the appropriate load.

The orange wire that can be seen on the left side of Figure 25, comes from Figure 26, which will be explained next. Through this connection, the value that the load must have is transmitted.

Once the value of the desired load is known, which can be from 0.5Ω to 127.5Ω (progressively increasing 0.5Ω), the ModBus slave corresponding to the relay board must be informed, which switches must open or close to obtain the desired load by combining the available resistances.

All possible load values are ordered in an ascending list in an Excel file, which can be found in Appendix 2. Each possible value is assigned a decimal code, starting with 0.5 Ohms with decimal value 1, up to 127.5 Ohms with decimal value 255. The decimal value is obtained by simply multiplying the value of the resistor by two. This first step can be seen on the left side of block E.

Once the value of the resistor is converted to a decimal number, the next step is to convert it into binary code. With the binary codes, the combination of the switches that must be open in the relay board to obtain the desired load is obtained, using the 1 as an open switch and 0 as a short circuit.

By means of the divisions that can be observed after the previous step mentioned, and analysing the remaining of this division, it is decided if the switch has to be opened or closed. Through a code block and the if-else function, the remaining part is analysed, which if it is 1 or higher, corresponds to the value 511 (opens the breaker) and if not, to the value 512 (short circuit).

This information is communicated to the ModBus slave of the relays board, as well as indicating which switch is being referred to. The information about which switch should be operated is obtained simply by adding 1 to the loop iteration number since as it is known, the iterations start from 0. As a summary, the slave is informed at the same time, which switch should be operated (from 1 to 8) and the state it should have (open or short circuit).

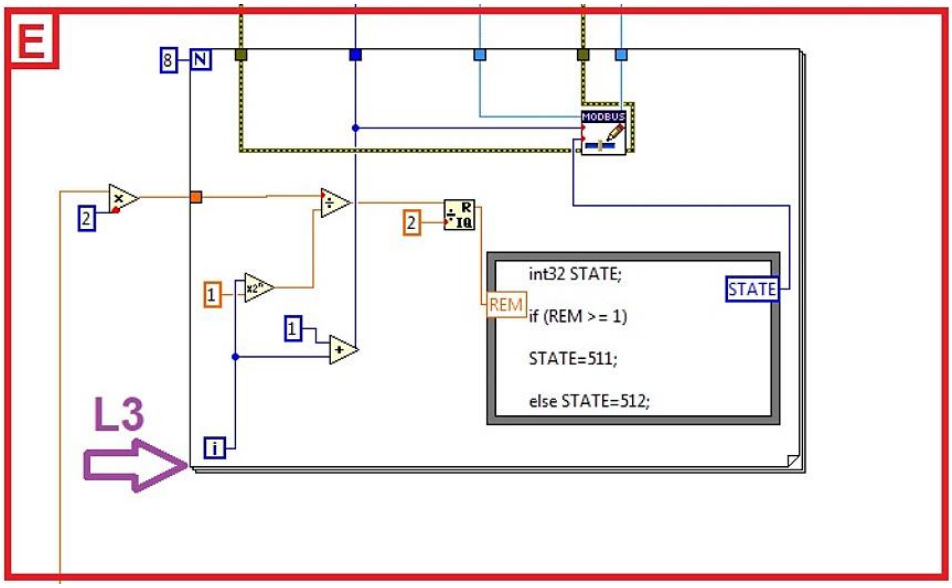

Figure 25: Detailed view of block E (Authors' own, 2020)

The load value, necessary for the above operations, is calculated from the data entered by the user in "Min resistor value" and "Step size".

Multiplying the value of the "Step size", by the number of iterations of the L2 loop, and adding the "Min resistor value", the value that the load must have is simply calculated. This value is updated each time the iteration number of the L2 loop increases.

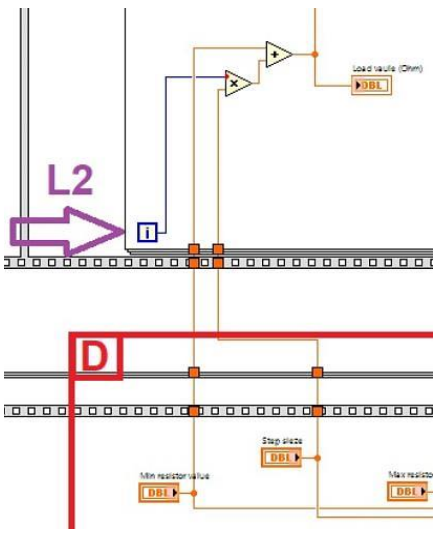

Figure 26: Load value calculation (Authors' own, 2020)

4.1.6. Block F - Data format converter

In block F, the data measured by the energy meter is read. On this occasion, the ModBus slave is used to read information generated by the device and not to run or control it as with the two previous slaves.

When the data of the energy meter is read by the slave, LabVIEW interprets it as an array of integers. In order for this data to be correctly interpreted to be operated and used later, it must be converted to scalar floating-point format due to it is the format that the energy meter uses. The colour and thickness of the wires indicate the format of the data. In Figure 31, from section 4.1.9. all wire types can be found.

The energy meter uses two 16-bit packets to send the 32-bit data. These 16-bit packets will also be read as integers by the LabVIEW program. To fix this issue, a conversion is needed.

First, the array size is read, then the array size is divided by two which sets a Boolean value that enables a “Case” structure. The case structure will be in “true” case when the reminder is equal to zero calculated by the “Quotient and reminder” function. This is done because data is spread in packets of two so to enable the conversion, the array needs to be multiple of two.

Inside that case structure, a “For loop” structure is used. The number of iterations to loop will be determined by the quotient of the previous operation. Onetime in the loop structure, two index arrays can be seen on which the data read by the slave will be its input data.

On the other hand, to select the index of the first index array, the iteration loop indicator will be doubled so the first 16-bit of each number to be read can be selected. For the second index array, the operation used for the previous index array is reused with the difference that the value of 1 is added to it so the second 16-bit of each number can also be selected properly.

After having the two 16-bit packets ordered, the functionality “Join numbers” is used to join them as a 32-bit and be ready to be converted to floating-point by the “Type cast” function. For a detailed view of these functions, check Figure 28.

Finally, the converted data is sent to block G.

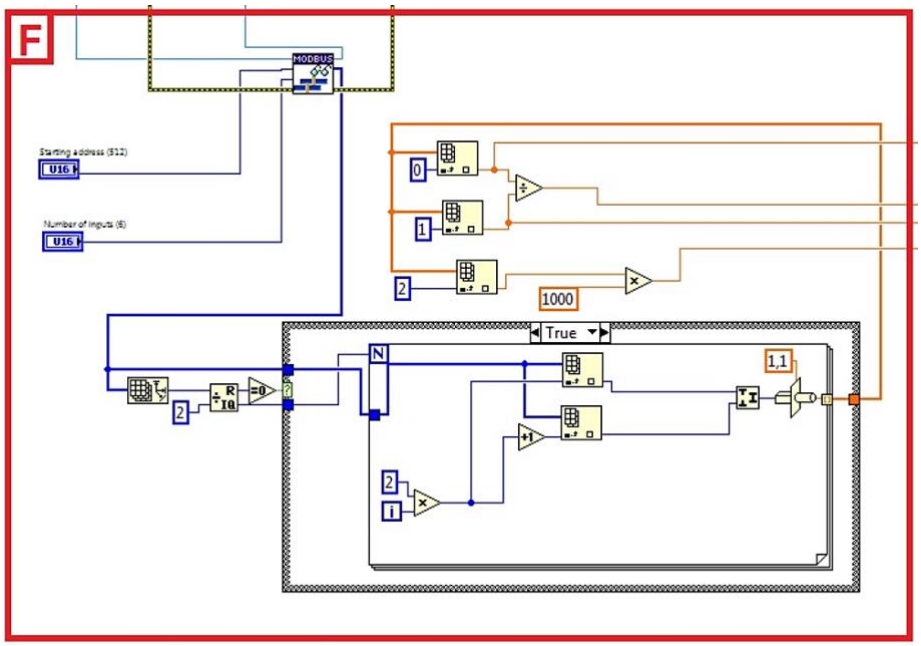

Figure 27: Detailed view of block F (Authors' own, 2020)

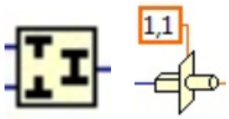

Figure 28: "Join numbers" and "Typecast" functions (Authors' own, 2020)

4.1.7. Block G - Data matrix generator

In block G, all the data to be displayed in the Excel file will be sorted. Therefore, an array of 5 values is initially created. The order and data of this array are as follows:

- Voltage (V)
- Current (A)
- Theoretical Load (Ohm) – [Load value reference calculated in block D]
- Measured Load (Ohm) – [Load obtained from Voltage/Current division]
- Power (W)

To enter the data correctly in Excel, the floating-point array must be converted to a string. This change can be seen when the wire turns to purple.

The data indicating the power of the floodlight is also needed. To do this, the reference value "FL value" obtained previously is used and is converted to a percentage using a rule of three. Like the previous array, this value is converted to "string" format and added to the "string" of 5 values in the first position, thus obtaining a string with the 6 values needed for the Excel

file (FL value (%) – Voltage (V) – Current (A) - Theoretical Load (Ohm) - Measured load (Ohm) – Power (W)).

The final string generated is sent to the H block. Also, the values of this string are sent to the property node that can be seen on the right side of the block. This node will be used to create the data table that is in the user's interface by creating a control on it. In Figure 35 from section 4.1.9. it is deepened on this element.

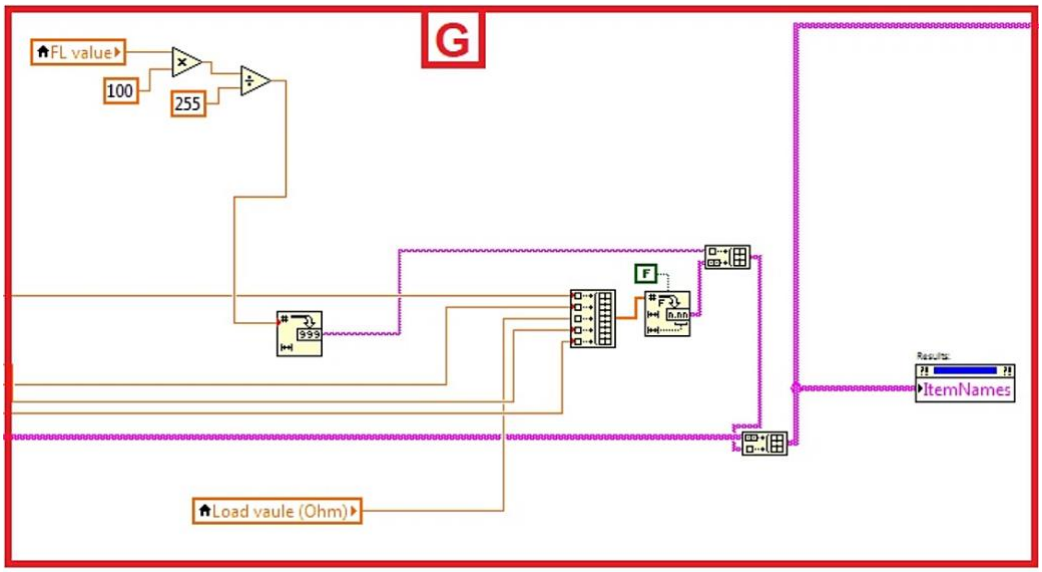

Figure 29: Detailed view of block G (Authors' own, 2020)

4.1.8. Block H - MS Excel report generator

Finally, in block H, the Excel file is generated with the data that has been generated in the previous blocks.

LabVIEW functions are used to create an Excel file and edit it as desired. The file receives as input data the strings of 6 elements and they are sorted in column mode. LabVIEW also allows editing the headers of these columns, which is what can be seen at the top of the H block in purple. Also, the file is configured so that it maximizes its screen once the total execution of the program is finished.

Therefore, when the Excel file is opened on the screen, it means that the execution of the program is over and it is time to analyze the results obtained with the tests performed.

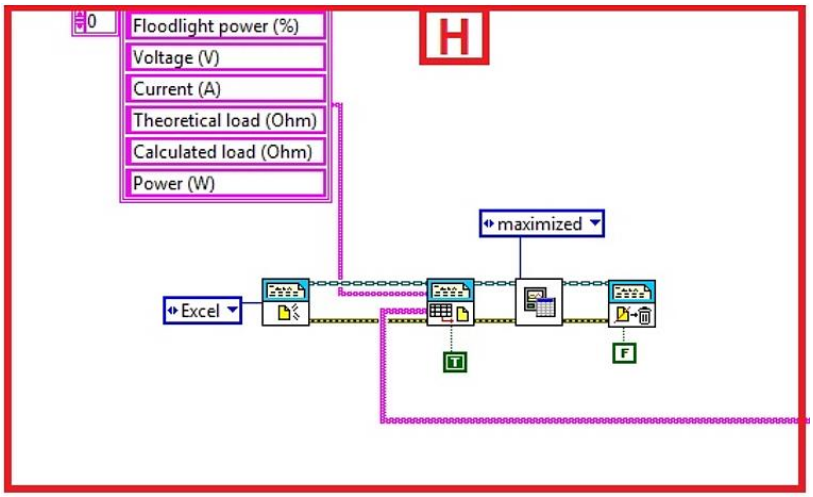

Figure 30: Detailed view of block H (Authors' own, 2020)

4.1.9. Details explanation

On this section, some important details will be explained that have not been discussed in the previous sections. Both functions which have not been deepened and functions that are not within any of the main blocks highlighted.

Different types of wires have been used on this program. They can be found in different colours and thicknesses depending on the data format it transmits. Note that LabVIEW sets the colour and the thickness automatically by detecting data format. Below is a picture with all wire types available in LabVIEW.

Figure 31: Wire types in LabVIEW (National Instruments, 2019)

Since only one USB to RS485 board is used to control different devices, a Unit ID must be defined for each slave. To set up it, a Property Node will be needed, which is shown in Figure 32.

Only two property nodes have been used because the Unit ID of one of the slaves is already preset in the ModBus master configuration. The node has been used to define the Unit ID of the slaves corresponding to the floodlight and the energy meter, while the Unit ID of the relay board is configured with the master.

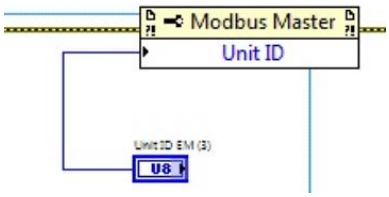

Figure 32: Property node – Unit ID selector (Authors' own, 2020)

For all three slaves used, a function is needed to indicate that the execution of the device is finished. This is done by using the "Shutdown VI" function shown in Figure 33. It is also needed to create an indicator that shows possible errors that could have occurred during execution.

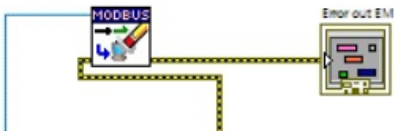

Figure 33: Slave shutdown (Authors' own)

In order to display the table with the measurements taken in real-time in the user interface, which can be seen in Figure 34, it is necessary to create a control on the property node of block G, which can be seen in Figure 35.

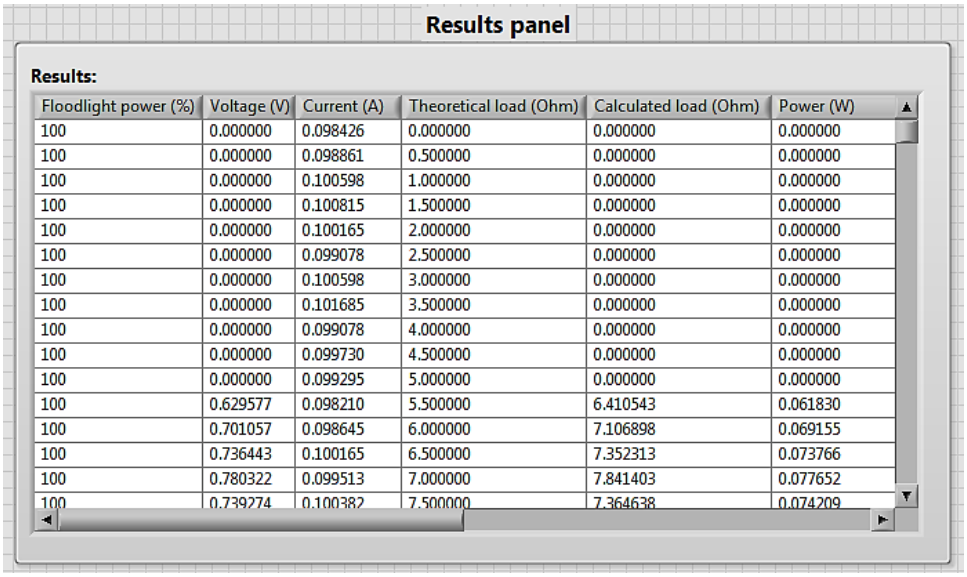

Floodlight power (%)	Voltage (V)	Current (A)	Theoretical load (Ohm)	Calculated load (Ohm)	Power (W)
100	0.000000	0.098426	0.000000	0.000000	0.000000
100	0.000000	0.098861	0.500000	0.000000	0.000000
100	0.000000	0.100598	1.000000	0.000000	0.000000
100	0.000000	0.100815	1.500000	0.000000	0.000000
100	0.000000	0.100165	2.000000	0.000000	0.000000
100	0.000000	0.099078	2.500000	0.000000	0.000000
100	0.000000	0.100598	3.000000	0.000000	0.000000
100	0.000000	0.101685	3.500000	0.000000	0.000000
100	0.000000	0.099078	4.000000	0.000000	0.000000
100	0.000000	0.099730	4.500000	0.000000	0.000000
100	0.000000	0.099295	5.000000	0.000000	0.000000
100	0.629577	0.098210	5.500000	6.410543	0.061830
100	0.701057	0.098645	6.000000	7.106898	0.069155
100	0.736443	0.100165	6.500000	7.352313	0.073766
100	0.780322	0.099513	7.000000	7.841403	0.077652
100	0.739274	0.100382	7.500000	7.364638	0.074209

Figure 34: Result's table on the user's interface (Authors' own, 2020)

Figure 35: Control of block's G property node (Authors' own, 2020)

For being able to transmit the information between loops, flat sequences and conditional blocks it is necessary to make use of nodes. The nodes that have been used in the program are those that can be seen in Figure 36.

The first node that can be observed (purple square) is used as a basic connection node, which sends the information to the next point once it is received. While the second one (purple square with an arrow) which is called "shift register" can store the information being generated in the loop, and not send it to the next point until the loop has performed all its iterations.

Summarizing, the first node sends the data to the next point with each iteration of the loop, while with the shift register the data generated in the loop is stored in it and it is not sent until the loop has been executed completely. For example, as it can be observed, the data of the G block is not sent to the Excel generator data by data, it is sent together once all the measurements are taken.

Figure 36: Types of nodes (Authors' own, 2020)

The complete program can be found in the following link:
https://drive.google.com/file/d/1banxN-iDZL-LMjnoszJi9I3eLyPSorhb/view?usp=sharing

4.2. Instructions for operating the program

After having properly assembled all the devices and ensured all the devices have power supply if they need it, so now the comparisons with the LabVIEW interface can be made.

Once seeing the user interface, it will be necessary to check the port where the ModBus device is connected to. To do that, go to “Device Manager” → “Ports” assuming the computer is running a Windows OS.

Then, as it can be seen in Figure 37, at the top of the user interface the ModBus parameters can be set. In the VISA resource name, the port where the Modbus device is connected should be selected. At the flow control box, none should be chosen and RTU should be set in serial type. The other parameters were previously configured in the Modbus Protocol configuration.

Below the parameters configuration panel, it can be found three more panels. One for each device; the floodlight control (FL), relays control (RE) and energy meter control (EM).

In the FL control, it can be chosen if the test is carried out with 4 different light stages (25% - 50% - 75% and 100% of the power of the floodlight) or if it is just carried out at one stage, adjustable with the "Floodlight manual" button. In case a specific case wants to be selected, “Manual Floodlight” button has to be ON and set the value (from 0 to 255, assuming 255 will be the 100% of the power output of the floodlight) to the Floodlight value box. Unit ID = 1 as configured before and Address = 0 in case the DMX device is set to A001.

About the RE control, there is the possibility to choose the minimum load value to the maximum load value but also the step size that will be taken to go from the minimum to the maximum. Remind that Unit ID of the relays board was set to 2.

At the EM control box, Number of inputs = 6, Starting address = 512 and Unit ID = 3. By setting the number of inputs to 6 and the starting address to 512 means that it will read the addresses from 512 to 517. Addresses 512 and 513 correspond to the voltage, 514 and 515 to the current and 516 and 517 to the energy.

Note that all of the parameters are reminded between the parenthesis. This set up will only work if followed the device's configuration before and the COM port is the correct one.

Finally, at the bottom of the user’s interface, it can be seen a results table where the measures are taken will be seen in real-time. This table shows the floodlight power as a percentage, the voltage, the current, the theoretical load, the calculated load (by dividing voltage by current) and the power.

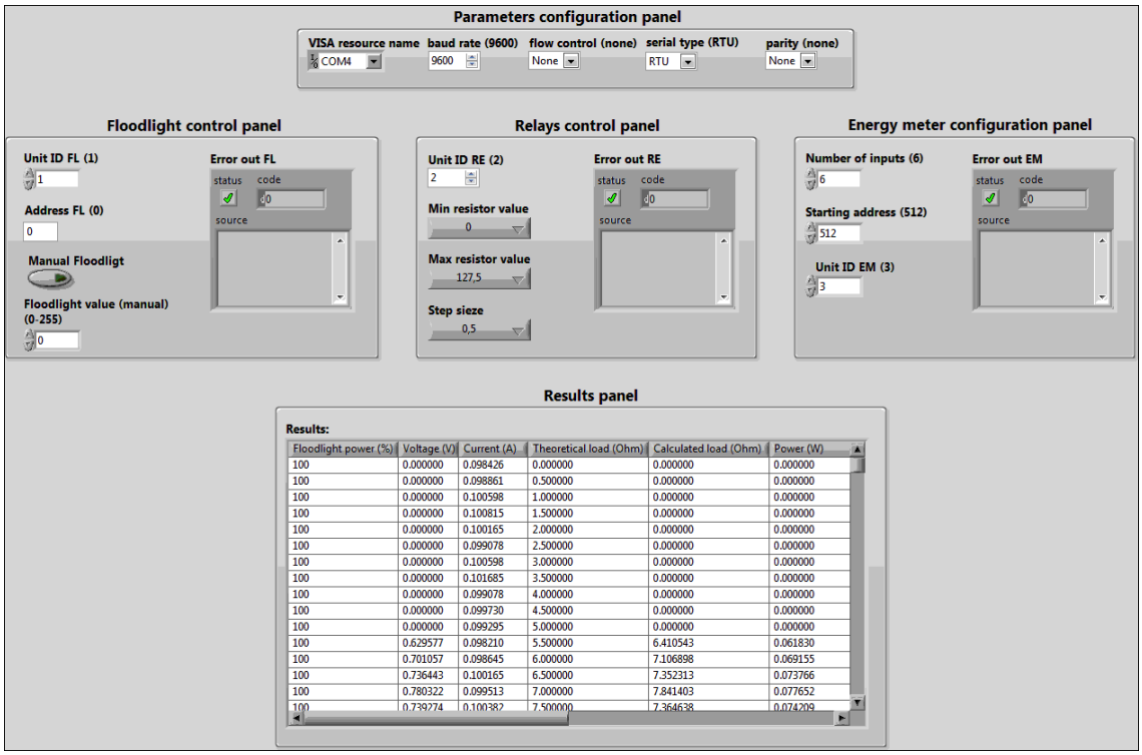

Figure 37: User interface (Authors' own, 2020)

5. Measurements and testing

Having assembled all the equipment, the tool will be tested by taking further measurements to later try to compare the solar panels and see if the efficiencies commented on 2.2 can be verified.

5.1. Summary of the tests performed

The amount of light registered in front of the panels when floodlight power output was at 100% was 40Klux. It is also important to remind that one of the thin-film used is a 35W PV panel meanwhile the others are 30W.

In Table 1 a summary of the tests carried out can be seen. To make the shadows, a cardboard rectangle has been used which has been moved as shown in the sketches. The dimensions of the cardboard are 70 x 4 cm.

Table 1: Summary of the taken tests (Authors' own, 2020)

NAME	SKETCH	SPECIFICATIONS
1st TEST		
Full test with no shadow		4 different light stages (25%, 50%, 75%, 100% floodlight power output), 255 load stages.
2nd TEST		
Test at 100% floodlight power output with no shadow		1 light stage (100% floodlight power output), 255 load stages.
3rd TEST		
Shadow bottom		1 light stage (100% floodlight power output), 255 load stages.
Shadow left	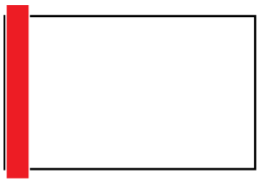	1 light stage (100% floodlight power output), 255 load stages.
Shadow middle horizontal		1 light stage (100% floodlight power output), 255 load stages.
Shadow middle vertical	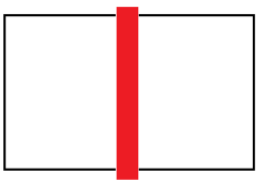	1 light stage (100% floodlight power output), 255 load stages.

Shadow right	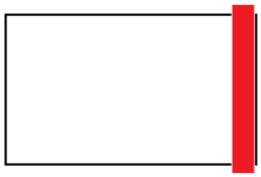	1 light stage (100% floodlight power output), 255 load stages.
Shadow top		1 light stage (100% floodlight power output), 255 load stages.

5.2. First test – No shadows and 4 light stages

The first test taken has been an execution of the program in "Automatic" mode running through all the load possibilities (from 0.5Ω to 127.5Ω increasing half Ohm each iteration) for each of the three different solar panels studied.

This test is carried out to document how the panels behave depending on the amount of light they are receiving so the automatic mode consists of 4 different light situations without shadows by reproductions 25%, 50%, 75% and 100% of the power output of the floodlight used.

The results obtained from the first test can be seen in

Figure 38, Figure 39, and Figure 40 which show the power-voltage graph corresponding to the monocrystalline panel, the 30W thin-film and the 35W thin-film panel in that order.

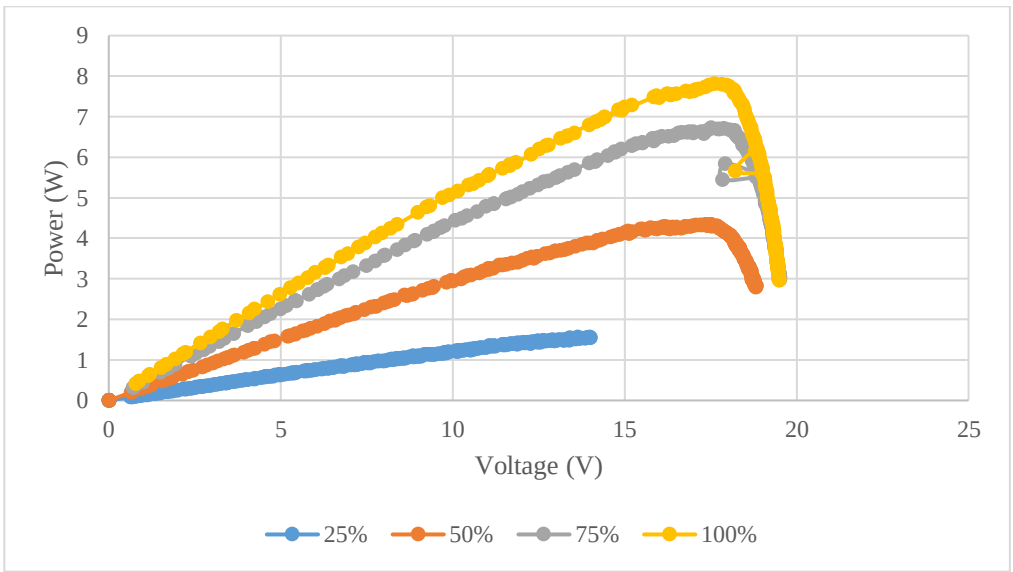

Figure 38: Monocrystalline over different light stages (Authors' own, 2020)

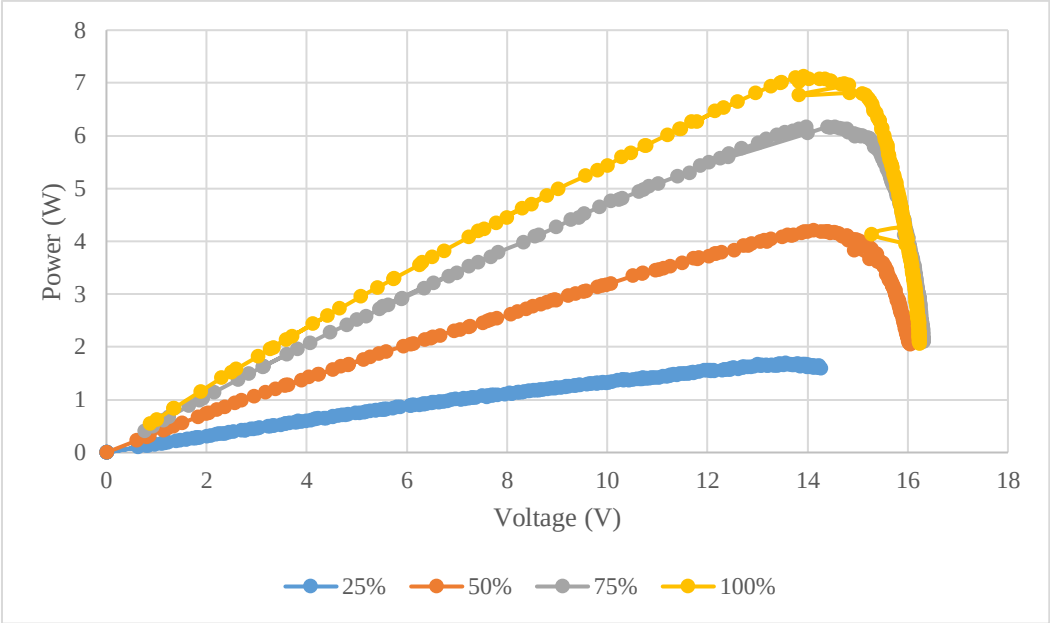

Figure 39: 30W thin-film over different light stages (Authors' own, 2020)

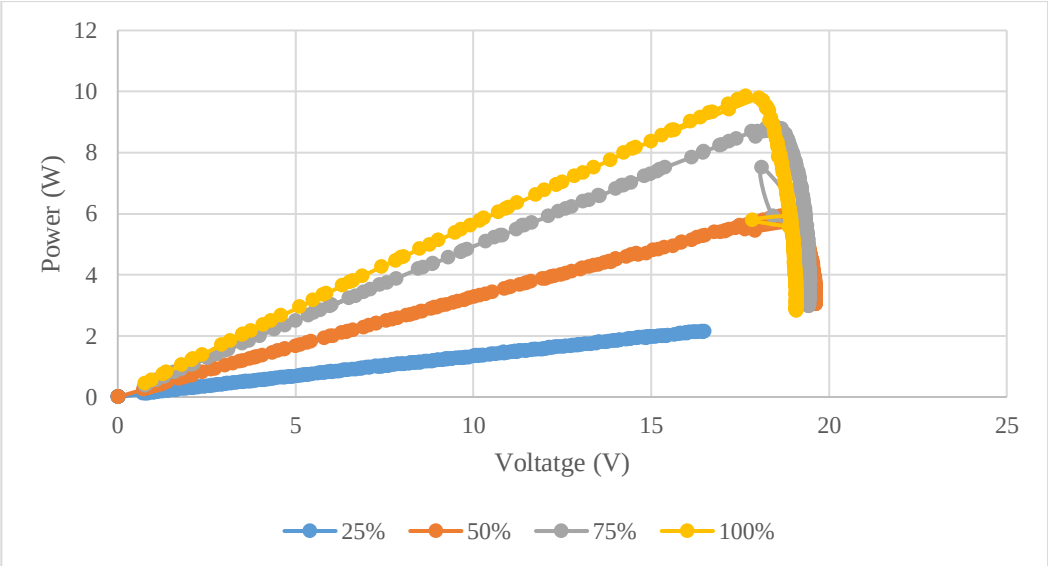

Figure 40: 35W thin-film over different light stages (Authors' own, 2020)

The graphs show no surprise as to what one might expect in terms of light power percentages, the higher the light output, the more power is obtained. Although it is important to note, that just after reaching the maximum power, the power decreases in a dive regardless of the percentage of light with which the test has been performed.

However, it is curious that in the three solar panels, normally, once the peak power has been exceeded, abnormal values can be seen. It is not known why this happens; it should be studied.

Taking into account the data of voltage, it can be concluded that the power peak is obtained with around 18V in the case of the monocrystalline panel and the 35W thin-film, independently of the percentage of light power. In the case of the 30W thin-film, the peak is obtained with about 14V, also independently of the light percentage.

The information provided by the data corresponding to the load indicates that the maximum power is obtained with nearby 30Ω in the case of both thin-film panels. With the monocrystalline panel, almost 40Ω are needed for reaching the maximum power. With the data obtained when testing these three panels, it can be concluded that in thin-film panels, a lower load is needed comparing to the monocrystalline to reach the peak power.

5.3. Second test – No shadows and 100% of light-power

The second tests performed were run over the "Manual" mode with 100% of floodlight power through all the 255 load possibilities for the three panels compared. This test can be used to make a comparison of the three panels considering the panels would be full sunlight with no shadows.

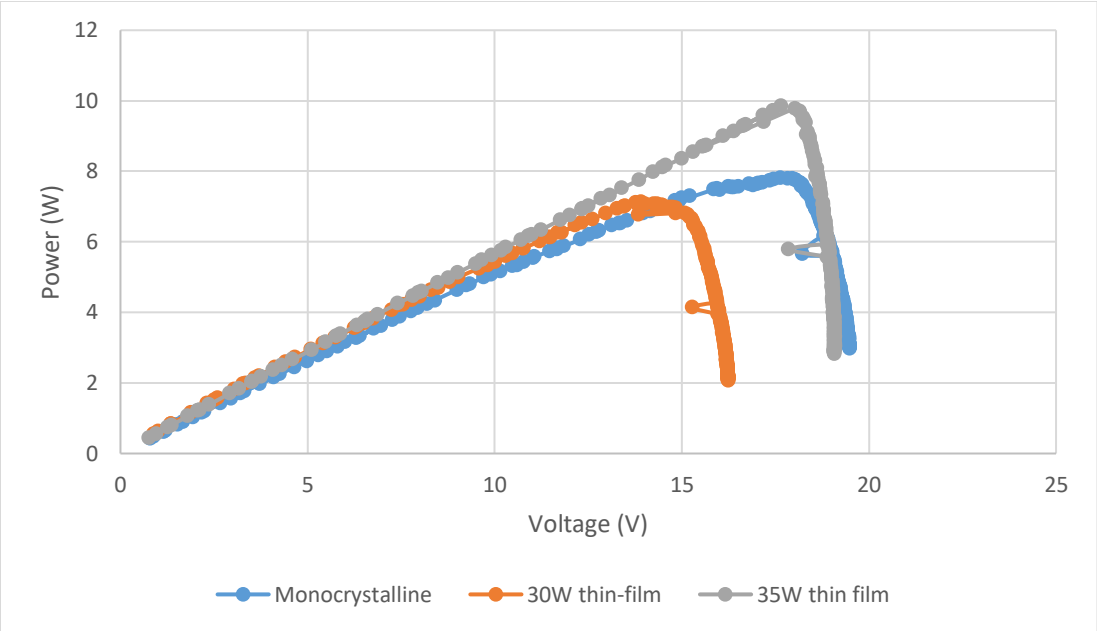

Figure 41: Comparison between the three PV panels (Authors' own, 2020)

An analysis of the results obtained in Figure 41, corresponding to the 30W monocrystalline panel, the 30W amorphous panel and the 35W amorphous panel, in that order, can be seen in Table 2.

Table 2: Contrasted data from the three solar panels (Authors' own, 2020)

Solar panel	Maximum power output (MPO)	Voltage generated at MPO	Matching load at MPO
MONOCRYSTALLINE 30W	7.81W	17.62V	39.75Ω
THIN-FILM 30W	7.12W	13.91V	27.18Ω
THIN-FILM 35W	9.85W	17.65V	31.62Ω

What is most striking when looking at the data provided in Table 2, is that the highest peak power is obtained with the 35W thin-film. Under equal conditions, i.e. if all the panels had the same power, the highest peak would be expected to be obtained with the monocrystalline panel.

There is a notable difference between the peaks, with a 2W difference between the peak of the 35W thin-film and the monocrystalline. Between the peaks of the mono and the 30W thin-film, the difference is quite minor, although it can be observed that to reach the peak a higher voltage is needed in the case of the monocrystalline.

It can be seen that the behaviour of the three panels is practically identical until 13.5V are reached. Up to this point, the power rise behaves in a linear way. Also, as discussed in test one above, after the power peak is reached, the power drops.

5.4. Third test – Shadows and 100% of floodlight power

Last taken test was executed with the same conditions as the previous one but shading some parts of the solar panels. When talking about output powers, reference is made to the maximum values of each situation unless otherwise stated.

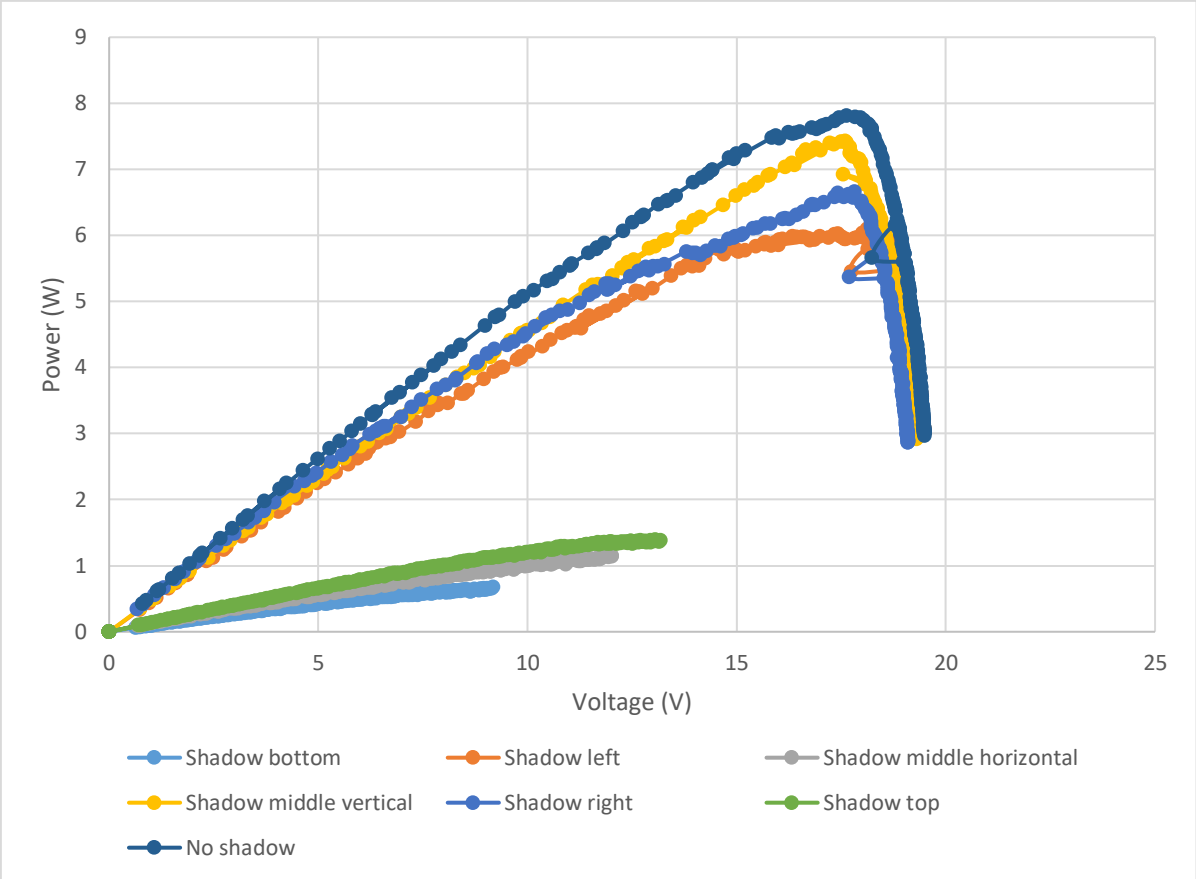

Figure 42: Comparison monocrystalline over different situations

When Figure 42 is observed, at first sight, it can be seen that there is a big difference between placing the cardboard that casts the shadow in a vertical or horizontal position.

When placed in a horizontal position the maximum power reached is only 1.38W when the cardboard is placed on top of the panel. It can be seen that the shading that affects most is if the bottom of the panel is covered.

When the cardboard is placed vertically, the difference compared to when there is no shadow is quite small, obtaining practically the same values when the cardboard is placed vertically in the middle of the panel. The peak obtained when there is no shadowing is 7.81W while when the cardboard is in the middle, the peak obtained is 7.66W, a practically negligible difference. As a percentage, by placing the cardboard horizontally, the power drops by 82.33% while by placing it vertically it drops by 1.92%.

It is interesting to note that the shadow affects the left side more than the right side of the panel.

It should be pointed out that when the cardboard is placed horizontally, it covers a larger surface than when it is placed vertically, due to the rectangular shape of the panel. However, the difference in the covered surface area does not justify the fact that horizontal shading produces so few power compared to vertical shading.

Deviations are still seen in some values once the power peak has been exceeded as discussed in the first test, in section 5.2.

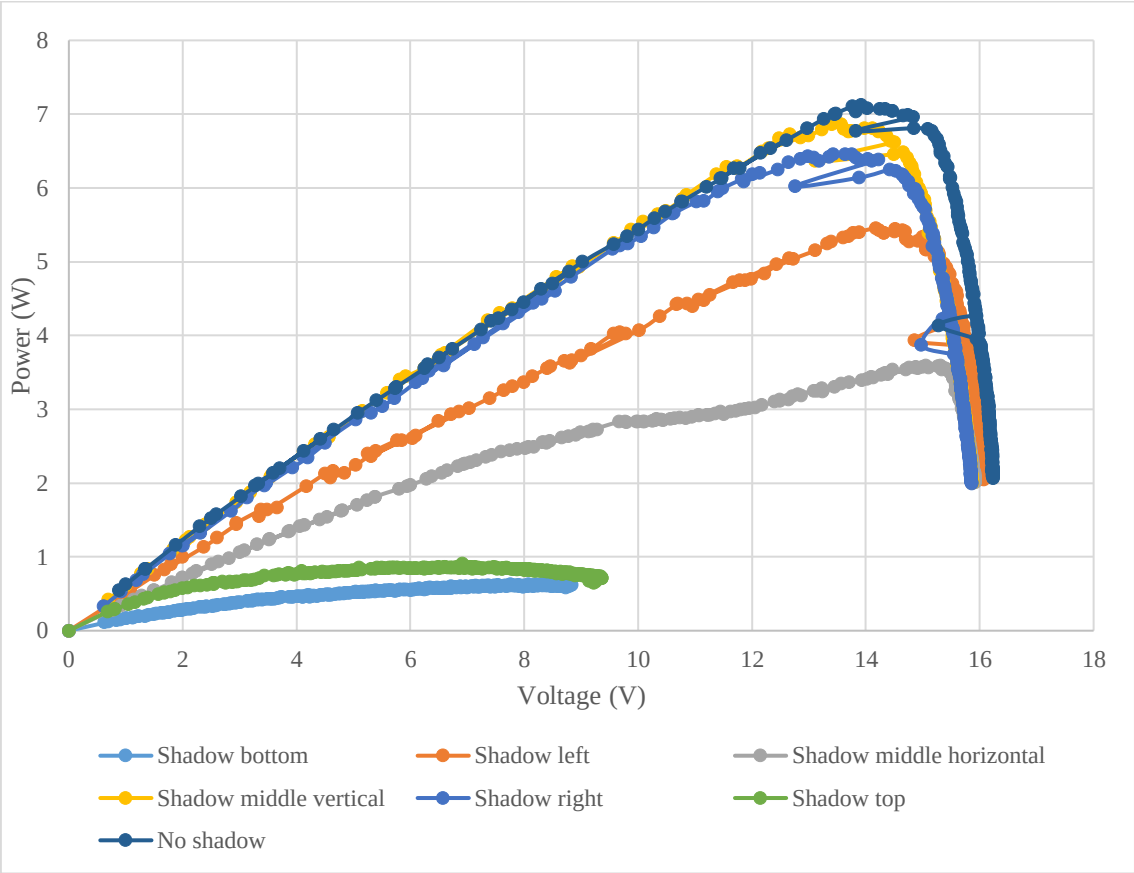

Figure 43: Comparison 30W thin-film over different situations

The results obtained when performing the shadow test with the 30W thin-film panel are generally quite similar to those of the monocrystalline panel. The behaviour of the curves, as with the previous panel, shows that the horizontal shading affects much more than the vertical shading.

In this case, when looking at the horizontal shading, a difference can be seen and is that when the cardboard is placed in the middle horizontally, the losses are much lower than if the cardboard is placed at the top or bottom. When the cardboard is in the middle, 3.57W are reached, which means a drop of 49.86% compared to when no shadow influences it, while with the cardboard at the top or bottom, not even 1W of power is reached, thus assuming a downturn of 85.96%.

When the vertical shading is observed, it can be seen that again as with the mono panel, when the cardboard is placed vertically in the middle, there is practically no difference from when there is no shade. It should be noted that with the right shading, the difference from the unshaded one is far less (-9.41%), while if the shading is placed on the left side the difference is greater (-23.88%), there being 1W difference between the peak of the right shading and the left one.

As for the values that come out of the trend of the curves, it can be seen that with the application of shade they have increased.

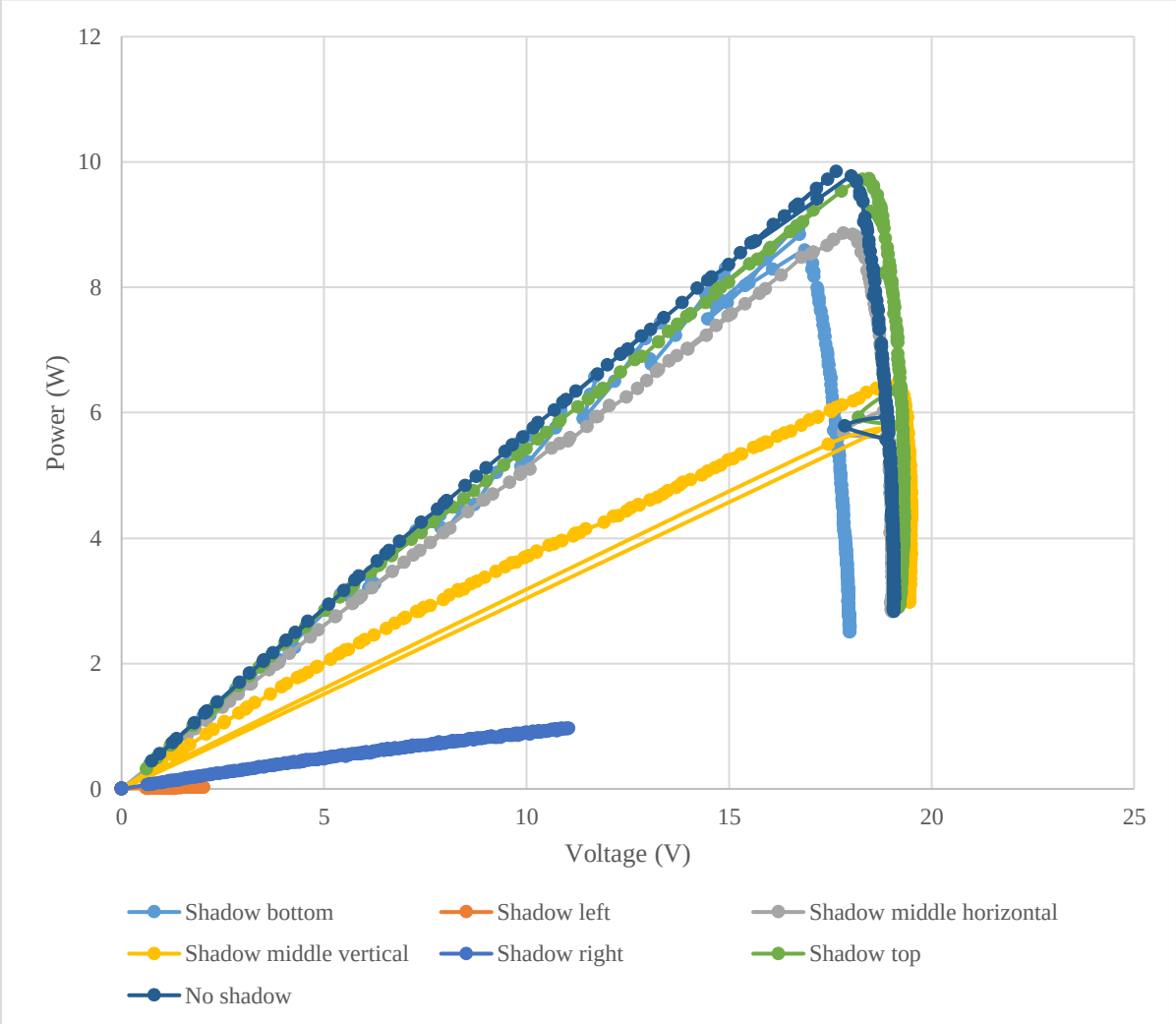

Figure 44: Comparison of 35W thin-film over different situations

Looking at Figure 44, it can be seen the shadows test outcome of the 35W thin-film solar panel in which it can be seen some differences compared to the two shadow tests commented above.

The first big difference is that this solar panel is affected many more by the vertical shadows than by the horizontal ones as was the case with the previous ones. Taking as example the middle horizontal and middle vertical curves, considering that are the ones with less difference, the power output of the solar panel with the cardboard placed vertically is 6.43W meanwhile when placing the cardboard horizontally, the power output reaches 8.86W. Compared to when there is no shadow, it is seen that when shading vertically, the output power is affected by -34.72% meanwhile when shading horizontally, the output power is affected by -10.05%.

The other difference to consider is that by looking at the curves that are closest to the no shadow curve, it can be seen that unlike the other comparisons, the shadows in the middle of the panel produce more losses than on the top or the bottom of it. In that case, the panel is capable of giving a power output of 9.73W when the cardboard is placed on the top and 8.94W when placed on the bottom. Bearing in mind that the maximum power output reached with no shadow is 9.85W the impact is -1.22% for the shadow on the top and -9.24% for the shadow on the bottom.

Moreover, it stands out that when the shadowing it is placed on the left side of the panel, the power outcome is near 0W. This factor could be produced because of the way that the panel is built inside.

Returning to the aspect of the deviations that are seen when overcoming the power peak, it can be seen that in this case apart from increasing the number of deviations it is also seen that these deviations have increased greatly.

In Table 3 it can be seen a summary of the effect of the shadow on each panel. It is compared the output obtained when the panel is at its maximum and minimum effect by the shadow with the output obtained without shadows.

Table 3: Comparison of the shadowing effect

Solar panel	Most sensible area to shadowing Impact (%)	Less sensible area to shadowing Impact (%)	Maximum power output without shadowing
MONOCRYSTALLINE 30W	Shadow bottom -91.34%	Shadow middle vertical -4.84%	7.81W
THIN-FILM 30W	Shadow bottom -91.09%	Shadow middle vertical -3.56%	7.12W
THIN-FILM 35W	Shadow left -99.66%	Shadow top -1.18%	9.85W

6. Discussion

With respect to the initial aims and objectives, the main goal of the thesis has been strongly achieved by being able to create a didactic tool which allows the automatic testing of PV panels. The final result obtained, as far as the creation of the program is concerned, has been satisfactory, having managed to implement all the functions and modes that had been proposed for the creation of this user-friendly yet useful tool.

The tool has been successfully implemented with the automatic switch of the relays depending on the load desired to be set. Also, the results can be seen in real-time at the user's interface of the LabVIEW program while executing as well as all the results are exported to an excel file where graphs and comparisons can be made easily. Besides, detailed documentation of assembling and the programming has also bee included so it can be used as a manual for anyone interested in using that utensil.

Different shading scenarios have been prepared and executed so the tool could be tested while panels tested could be better compared. It can be said the objectives have been successfully met.

With respect to the results obtained in the tests carried out, interesting data have been found, of which the most relevant will be commented on next. It has been demonstrated and researched how a shadow of equal dimensions can affect in different ways depending on which part of the panel that shadow is located.

It should also be noted that there is no significant difference in the output obtained by monocrystalline and thin-film 30W panels with the premise that the monocrystalline is theoretically more efficient than thin-film. It should be noted that the input they have undergone has been limited by the power of the floodlight.

The discovery that stands out the most, with respect to the positioning of the shading, has been in the case of the 35W thin-film solar panel when the panel has been covered vertically. It has been possible to verify that if the left side of the panel is covered, the energy generated is practically null, while if the same surface is covered, but on the opposite side; the right side, the energy generation is very similar to that obtained when the panel is completely uncovered.

Continuing to analyze the effect of shading on the solar panels, there are great differences in the behaviour of these, which are interesting to comment on. For both the monocrystalline panel and the 30W thin-film, positioning the shadow horizontally is more detrimental for the panel. As for the monocrystalline, it is very harmful regardless of the height of the shadow while for the 30W thin-film, if positioned in the centre, is less harmful when it comes to producing energy. In contrast, the 35W thin-film acts differently than the previous two; they are more affected by vertical shadows as mentioned above.

These differences that occur in the generation of energy when varying the shading can be produced by the way the internal connections of the panel are made. Studying and analyzing the internal connections of the solar panels is a very interesting study that could be done to try to understand why this happens.

These effects could be explained by how the cells within each solar panel are connected to each other. According to (Brown, 2016), that uses an analogy of water flowing through a pipe, says that the flow rate of water through the pipe is constant, much like the current through a cell string is constant for a given irradiance level.

The shadow of a solar cell is similar to the introduction of a clog into a water pipe. Pipe obstruction restricts the flow of water throughout the pipe. Similarly, when a solar cell is shaded, the current is reduced throughout the chain.

The reduction of energy varies depending on how many cells are included and the cell combinations. In a study conducted on 2017 (Kazem, et al., 2017), the experimental results show that the largest decrease in the output voltage of a polycrystalline PV occurs when parallel combinations of a PV cell are covered by shadows. It is assumed that both monocrystalline and amorphous will behave in a similar manner. At the same time, the smallest reduction occurred when the cells involved in series connection. When nine cells in series were covered, the output dropped to approximately 2V (concerning to time), but when four arrays of cells in parallel were covered, it fell to almost 6V. This shows that it is important to compare the effects of shadows in connection with the combinations of cells covered.

With respect to the limitations of the work, the biggest drawback has been to continue with the thesis while facing the global COVID-19 pandemic. Due to it, the laboratory where the project was been carried out was closed so consequently, a laboratory had to be improvised in the apartment.

It is important to consider that all the measurements were taken indoor and not at the same time, so it could be that the amount of ambient light was not exactly the same on each measurement, but just in case, the differences should not be much important. In addition, better materials such as a more powerful floodlight could have been used, to have been able to at least simulate the average equivalent of lux found on a typical sunny day. Also, the impossibility of not being able of disposing of a polycrystalline solar panel has been a weak point for this study as the quality of the comparisons would have increased in the case of having the three types of solar panels with more presence in the current market.

With respect to the inconsistencies, the lack of experience and practice with the LabVIEW program, the ModBus Protocol as well as with some of the devices used slowed down the process. At the same time, the aim of enlarging our knowledge and gaining practical experience was being accomplished. The thesis carried out by Victor Resa last year has been of great help in understanding the operation of the LabView program, especially with regard to the functions that encompass the ModBus protocol. Besides, several internet forums have been helpful, such as the official National Instruments portal.

With respect to consistencies, thanks to the knowledge in electronics, programming and renewable energies acquired in other engineering courses it has been easier to solve the different problems that presented while developing the project. Moreover, the knowledge provided by Hans Lindén has been of great help, especially concerning to the ModBus Protocol.

7. Conclusion

As solar panel technology is constantly evolving, it is important to keep researching on all the available possibilities to be able to get the maximum benefit of the sun, the most powerful source at humanity disposal.

It was possible to see how each panel studied behaved facing the different situations proposed. When choosing a solar panel, the tool developed can be very helpful if the system and the environment in which it will be installed is known because there is no single best panel, but depending on the situation one type of panel may be more suitable than another.

The tool has behaved correctly during all the tests carried out. No anomalies have been observed, except for some deviant values, although this does not affect the overall result of the test.

Several tests have been carried out simulating different shading situations, however, this tool allows the user to perform any type of test wished. The main objective was simply to create this automatic tool, but also to learn to analyse and discuss the output results. The tests carried out indicated that the panel type and orientation of shading with respect to the panel have a profound impact on electrical output and efficiency. Depending on the position of the shadow, the impact on the output power for the same solar panel can be from -1% to -99%.

Future research could be conducted to implement the tests on improved scenarios. One example could be trying to adjust the light source to be as similar as possible to the one the sun emits maybe by combining halogen technology with led technology. Further interesting research would be studying how the temperature of the panel surface affects the efficiency of it. Additional study could be undertaken to expose the panels to simulated ‘real-world’ conditions such as dirt on the panel, humidity in the environment or on the surface of the panels.

This project has allowed entering the world of renewable energies, whilst further deepening and improving practical knowledge both in the programming of automated processes and in the assembly of electronic circuits.

8. References

Accuenergy, 2018. *Acu DC 240 Power Energy Meter User Manual*, s.l.: s.n.

Ameri, T., Dennler, G., Lungenschmied, C. and Brabec, C. J., 2009. *Royal Society of Chemistry.* [Online]
Available at: https://pubs.rsc.org/en/content/articlehtml/2009/ee/b817952b
[Accessed 30 Jan 2020].

Anon. - Modified by authors, 2020. *canton-electronics.com.* [Online]
Available at: http://www.canton-electronics.com/mcu-relay-controller-c-53/uart-relay-modules-c-53_54/8-channel-dc-12v-rs485-relay-module-modbus-rtu-485-remote-control-switch-for-plc-ptz-camera-security-monitoring-p-943.html
[Accessed 19 May 2020].

Anon., 2019. *Bp.com.* [Online]
Available at: https://www.bp.com/content/dam/bp/business-sites/en/global/corporate/pdfs/energy-economics/statistical-review/bp-stats-review-2019-renewable-energy.pdf
[Accessed 12 Mar 2020].

Anon., 2020. *Iea.blob.core.windows.net.* [Online]
Available at: https://iea.blob.core.windows.net/assets/cf477276-f5a5-4130-9395-138035363668/Renewables-2019-Launch-Presentation.pdf
[Accessed 19 May 2020].

Anon., 2020. *Ise.fraunhofer.de.* [Online]
Available at:
https://www.ise.fraunhofer.de/content/dam/ise/de/documents/publications/studies/Photovoltaics-Report.pdf
[Accessed 3 Feb 2020].

Brown, 2016. *Shade Losses in PV Systems, and Techniques to Mitigate Them, Blog.aurorasolar.com.* [Online]
Available at: https://blog.aurorasolar.com/shading-losses-for-pv-systems-and-techniques-to-mitigate-them/
[Accessed 27 July 2020].

Choosing the Right Solar Panel for Your Rooftop, 2017. *SaveGeo.* [Online]
Available at: http://www.savegeo.com/choosing-right-solar-panel-rooftop/
[Accessed 19 May 2020].

Could DYE Transform into a “Mini-Tesla” of Solar?, 2016. [Online]
Available at: https://www.nexttechstock.com/dye-transform-mini-tesla-solar/
[Accessed 29 Jan 2020].

End-of-life management Solar Photovoltaic Panels, 2016. *IRENA.* [Online]
Available at: https://www.irena.org/publications/2016/Jun/End-of-life-management-Solar-Photovoltaic-Panels
[Accessed 25 Jan 2020].

Fthenakis, et al., 2008. *ACS Publications.* [Online]
Available at: https://pubs.acs.org/doi/full/10.1021/es071763q
[Accessed 25 Jan 2020].

GreenMatch, 2020. *Greenmatch.* [Online]
Available at: https://www.greenmatch.co.uk/blog/2015/09/types-of-solar-panels
[Accessed 29 Jan 2020].

GreenMatch, 2020. *GreenMatch - Solar Battery Storage.* [Online]
Available at: https://www.greenmatch.co.uk/blog/2018/07/solar-battery-storage-system-cost
[Accessed 20 Mar 2020].

How Do Solar Panels Work?, 2016. *Solargain.* [Online]
Available at: https://www.solargain.com.au/blog/how-do-solar-panels-work
[Accessed 22 Jan 2020].

IENE Institute of Energy for South-East Europe, 2020. *IENE Institute of Energy for South-East Europe.* [Online]
Available at: http://www.iene.eu/irena-forecasts-59-solar-pv-price-reduction-by-2025-p2740.html
[Accessed 18 Mar 2020].

Kazem, et al., 2017. *Effect of Shadows on the Performance of Solar Photovoltaic (researchgate.net).* [Online]
Available at: https://www.researchgate.net/publication/311608006_Effect_of_Shadows_on_the_Performance_of_Solar_Photovoltaic
[Accessed 27 Jul 2020].

National Instruments, 2019. *Meaning of Different Wire Colors in LabVIEW - National Instruments.* [Online]
Available at: https://knowledge.ni.com/KnowledgeArticleDetails?id=kA00Z0000019LsVSAU&l=fi-FI
[Accessed 26 Apr 2020].

PVinsights, 2020. *PVinsights.* [Online]
Available at: http://pvinsights.com/
[Accessed 20 May 2020].

Renewable Energy World, 2017. *Renewable Energy World.* [Online]
Available at: https://www.renewableenergyworld.com/2017/01/26/solar-boom-5-leading-

reasons-for-the-industry-s-growth/#gref
[Accessed 20 Mar 2020].

RESI - Modified by authors, 2015. *Shop.marcomweb.it.* [Online]
Available at: https://shop.marcomweb.it/images/stories/virtuemart/product/resi-ds-dmx-modbus-e10.pdf
[Accessed 10 Apr 2020].

Ritchie and Roser, 2018. *Our World in Data.* [Online]
Available at: https://ourworldindata.org/energy
[Accessed 25 Jan 2020].

Solar energy generation, 2019. *ourworldindata.org.* [Online]
Available at: https://ourworldindata.org/grapher/installed-solar-PV-capacity?tab=chart&country=FIN+DNK+NOR+SWE
[Accessed 19 May 2020].

Stairville DMX Terminator XLR 3-Pol, M. T., 2020. [Online]
Available at: https://www.thomann.de/gb/stairville_dmx_endstecker_xlr_3pol.htm
[Accessed 9 Apr 2020].

Student Energy, 2020. [Online]
Available at: https://www.studentenergy.org/topics/solar-pv
[Accessed 21 Jan 2020].

SURFACE Syracuse University, 2020. *SURFACE Syracuse University.* [Online]
Available at: https://surface.syr.edu/cgi/viewcontent.cgi?article=1046&context=phy
[Accessed 29 Jan 2020].

The photovoltaic effect | PVEducation, 2020. *pveducation.org.* [Online]
Available at: https://www.pveducation.org/pvcdrom/solar-cell-operation/the-photovoltaic-effect
[Accessed 20 May 2020].

United Nations Climate Change, 2020. *United Nations Climate Change.* [Online]
Available at: https://unfccc.int/process-and-meetings/the-paris-agreement/the-paris-agreement
[Accessed 18 Mar 2020].

User's manual energy meter AcuDC 240 Series - Modified by authors, 2018. *Accuenergy.com.* [Online]
Available at: https://www.accuenergy.com/wp-content/uploads/AcuDC-240-Power-Energy-Meter-User-Manual.pdf
[Accessed 19 May 2020].

User's manual energy meter AcuDC 240 Series, 2018. *Accuenergy.com.* [Online]
Available at: https://www.accuenergy.com/wp-content/uploads/AcuDC-240-Power-

Energy-Meter-User-Manual.pdf
[Accessed 10 Apr 2020].

WebFX Solar Marketing, 2020. *WebFX Solar Marketing.* [Online]
Available at: https://www.webfx.com/industries/home-repair/solar/
[Accessed 20 Mar 2020].

Wikimedia Commons, 2013. *Wikimedia Commons*. [Online]
Available at: https://commons.wikimedia.org/wiki/File:Swanson_effect.svg
[Accessed 19 Mar 2020].

XLR-3, 2020. *wikipedia.org.* [Online]
Available at: https://es.wikipedia.org/wiki/XLR-3#/media/Archivo:XLR_pinouts.svg
[Accessed 9 Apr 2020].

Appendix 1: List of materials used I

NAME	MANUFACTURER	MODEL	DESCRIPTION	PRICE	LINK	IMAGE
Halogen floodlight	FAITHFULL	FPPSL1000CT	Floodlight that provides illumination from twin 500-watt lamps mounted on a sturdy telescopic stand that enables the lamp height to be adjusted between 78 cm and 183 cm. 1000 W. 1.9 m of cable length.	27€	https://www.shop.niceic.com/4608-Faithfull-FPPSL1000CT-Sitelight-Twin-Adjustable-Stand-1000-Watt-240-Volt	
DMX control dimer	Stairville	DS-2 RF DMX	DMX control dimer that enables setting the output power which also can be set as a switch pack. Dimensions: 182 x 92 x 65 mm.	55€	https://www.thomann.de/es/stairville_ds2_rf_dmx_1ch_dimmer.htm?ref=intl&shp=eyJjb3VudHJ5IjoiZXMiLCJjdXJyZW5jeSI6IjIiLCJsYW5ndWFnZSI6ImVzIn0%3D	

DMX to ModBus converter	RESI	RESI-DMX-MODBUS	RESI-DMX-MODBUS is a standard developed for communication between the console and the dimer. Dimensions: 17.7 x 90 x 58 mm.	178€	https://shop.marcomweb.it/en/shop-online/fieldbus/modbus-tcp-rtu/dmx512-modbus-rtu-ascii-converter-dettagli.html	
Monocrystalline PV panel	Victron energy	SPM30-12/3a	30 Watt Victron energy monocrystalline solar PV panel. Dimensions: 430 x 545 x 25 mm.	54€	https://www.sunstore.co.uk/product/12v-30w-monocrystalline-solar-panel/	
Amorphous PV panel	SOLARXON	ES-30W	30 Watt solar PV panel. Dimensions: 310 x 550 x 3 mm.	49€	https://www.thermosun.fi/epages/thermosun.sf/fi_FI/?ObjectPath=/Shops/Kuvaus/Products/100005	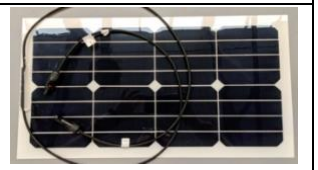

Amorphous PV panel	NORDMAX	NM35WFL	35 Watt NORDMAX thin-film PV panel with monocrystalline solar cells. Dimensions: 700 x 350 x 2.5 mm.	59€	https://www.aurinkopaneelikauppa.fi/epages/aurinkopaneelikauppa.sf/en_GB/?ViewObjectPath=%2FShops%2F20120903-11092-142553-1%2FProducts%2F02V35	
USB to RS485 board	FTDI and RS485 board manufactured at NOVIA	USB-COM485-Plus1 + RS485 board	A board that allows connecting from USB-B to an RS485 wiring module.	25€	https://www.digikey.fi/product-detail/en/ftdi-future-technology-devices-international-ltd/USB-COM485-PLUS1/768-1038-ND/2139300	
Energy meter	ACCUENERGY	AcuDC 243	Capable of metering DC voltage, current, power and energy. Features a built-in MODBUS RTU. Dimensions: 72 x 72 x 64.5 mm.	340€	https://www.powermeterstore.com/product/accuenergy-acudc-243-1000v-a2-p1-x5-c-d-dc-power-meter	

Resistors	ARCOL	HS50	Aluminium housed power resistors. Designed for direct heatsink mounting with thermal compound to achieve maximum performance.	41€	https://www.starelec.fi/index.php?cPath=49_101_269	
Relays board	Unbranded	R421A08	8 channel ModBus relay module equipped with mature and stable 8-bit MCU and RS485 level communication chip, adopts standard MODBUS RTU format RS485 communication protocol. Dimensions: 90 x 62 x 19 mm.	16€	http://www.icstation.com/channel-rs485-multifunctional-delay-relay-module-modbus-controller-p-14148.html	
Lever nuts	WAGO	221 family	Compact splicing connector with operating levers and transparent housing. Dimensions: 18.7 x 8.3 x 18.6 mm.	8€	https://www.wago.com/us/wire-splicing-connectors/compact-splicing-connector/p/221-413	

Wires	DONAU	D118	Coper conductor of 0.14mm2 with PVC isolation and an operating voltage of 60V. Max capacity of 1.5A.	>10€	https://www.starelec.fi/index.php?cPath=79_587_4001	
Power supplier (x2)	TENMA	72-2540	Programmable DC power supply.	108 €/unit	https://uk.farnell.com/tenma/72-2540/power-supply-1ch-30v-5a-prog/dp/2445412?ost=72-2540	

The document consists of 8 pages. The whole document can be checked on excel at the following link:
https://drive.google.com/file/d/1Q_YKz64vOaCJLEGQVFphcDeQL3-jG2_7/view?usp=sharing

Relay number	8	7	6	5	4	3	2	1		Binary code								Decimal code
Resistor value	64	32	16	8	4	2	1	0,47	Resistance	8	7	6	5	4	3	2	1	
	short	short	short	short	short	short	short	open	0.47								1	1
	short	short	short	short	short	short	open	short	1							1	0	2
	short	short	short	short	short	short	open	open	1.47							1	1	3
	short	short	short	short	short	open	short	short	2						1	0	0	4
	short	short	short	short	short	open	short	open	2.47						1	0	1	5
	short	short	short	short	short	open	open	short	3						1	1	0	6
	short	short	short	short	short	open	open	open	3.47						1	1	1	7
	short	short	short	short	open	short	short	short	4					1	0	0	0	8
	short	short	short	short	open	short	short	open	4.47					1	0	0	1	9
	short	short	short	short	open	short	open	short	5					1	0	1	0	10

short	short	short	short	open	short	open	open	5.47			1	0	1	1	11
short	short	short	short	open	open	short	short	6			1	1	0	0	12
short	short	short	short	open	open	short	open	6.47			1	1	0	1	13
short	short	short	short	open	open	open	short	7			1	1	1	0	14
short	short	short	short	open	open	open	open	7.47			1	1	1	1	15
short	short	short	open	short	short	short	short	8	1	0	0	0	0		16
short	short	short	open	short	short	short	open	8.47	1	0	0	0	1		17
short	short	short	open	short	short	open	short	9	1	0	0	1	0		18
short	short	short	open	short	short	open	open	9.47	1	0	0	1	1		19
short	short	short	open	short	open	short	short	10	1	0	1	0	0		20
short	short	short	open	short	open	short	open	10.47	1	0	1	0	1		21
short	short	short	open	short	open	open	short	11	1	0	1	1	0		22
short	short	short	open	short	open	open	open	11.47	1	0	1	1	1		23
short	short	short	open	open	short	short	short	12	1	1	0	0	0		24
short	short	short	open	open	short	short	open	12.47	1	1	0	0	1		25

short	short	short	open	open	short	open	short	13		1	1	0	1	0	26
short	short	short	open	open	short	open	open	13.47		1	1	0	1	1	27
short	short	short	open	open	open	short	short	14		1	1	1	0	0	28
short	short	short	open	open	open	short	open	14.47		1	1	1	0	1	29
short	short	short	open	open	open	open	short	15		1	1	1	1	0	30
short	short	short	open	open	open	open	open	15.47		1	1	1	1	1	31
short	short	open	short	short	short	short	short	16	1	0	0	0	0	0	32
short	short	open	short	short	short	short	open	16.47	1	0	0	0	0	1	33
short	short	open	short	short	short	open	short	17	1	0	0	0	1	0	34
short	short	open	short	short	short	open	open	17.47	1	0	0	0	1	1	35
short	short	open	short	short	open	short	short	18	1	0	0	1	0	0	36
short	short	open	short	short	open	short	open	18.47	1	0	0	1	0	1	37
short	short	open	short	short	open	open	short	19	1	0	0	1	1	0	38
short	short	open	short	short	open	open	open	19.47	1	0	0	1	1	1	39
short	short	open	short	open	short	short	short	20	1	0	1	0	0	0	40

short	short	open	short	open	short	short	open	20.47	1	0	1	0	0	1	41
short	short	open	short	open	short	open	short	21	1	0	1	0	1	0	42
short	short	open	short	open	short	open	open	21.47	1	0	1	0	1	1	43
short	short	open	short	open	open	short	short	22	1	0	1	1	0	0	44
short	short	open	short	open	open	short	open	22.47	1	0	1	1	0	1	45
short	short	open	short	open	open	open	short	23	1	0	1	1	1	0	46
short	short	open	short	open	open	open	open	23.47	1	0	1	1	1	1	47
short	short	open	open	short	short	short	short	24	1	1	0	0	0	0	48
short	short	open	open	short	short	short	open	24.47	1	1	0	0	0	1	49
short	short	open	open	short	short	open	short	25	1	1	0	0	1	0	50
short	short	open	open	short	short	open	open	25.47	1	1	0	0	1	1	51
short	short	open	open	short	open	short	short	26	1	1	0	1	0	0	52
short	short	open	open	short	open	short	open	26.47	1	1	0	1	0	1	53
short	short	open	open	short	open	open	short	27	1	1	0	1	1	0	54
short	short	open	open	short	open	open	open	28.47	1	1	0	1	1	1	55

short	short	open	open	open	short	short	short	28		1	1	1	0	0	0	56
short	short	open	open	open	short	short	open	28.47		1	1	1	0	0	1	57
short	short	open	open	open	short	open	short	29		1	1	1	0	1	0	58
short	short	open	open	open	short	open	open	29.47		1	1	1	0	1	1	59
short	short	open	open	open	open	short	short	30		1	1	1	1	0	0	60
short	short	open	open	open	open	short	open	30.47		1	1	1	1	0	1	61
short	short	open	open	open	open	open	short	31		1	1	1	1	1	0	62
short	short	open	open	open	open	open	open	31.47		1	1	1	1	1	1	63
short	open	short	short	short	short	short	short	32	1	0	0	0	0	0	0	64
short	open	short	short	short	short	short	open	32.47	1	0	0	0	0	0	1	65
short	open	short	short	short	short	open	short	33	1	0	0	0	0	1	0	66
short	open	short	short	short	short	open	open	33.47	1	0	0	0	0	1	1	67
short	open	short	short	short	open	short	short	34	1	0	0	0	1	0	0	68
short	open	short	short	short	open	short	open	34.47	1	0	0	0	1	0	1	69
short	open	short	short	short	open	open	short	35	1	0	0	0	1	1	0	70

short	open	short	short	short	open	open	open	35.47	1	0	0	0	1	1	1	71
short	open	short	short	open	short	short	short	36	1	0	0	1	0	0	0	72
short	open	short	short	open	short	short	open	36.47	1	0	0	1	0	0	1	73
short	open	short	short	open	short	open	short	37	1	0	0	1	0	1	0	74
short	open	short	short	open	short	open	open	37.47	1	0	0	1	0	1	1	75
short	open	short	short	open	open	short	short	38	1	0	0	1	1	0	0	76
short	open	short	short	open	open	short	open	38.47	1	0	0	1	1	0	1	77
short	open	short	short	open	open	open	short	39	1	0	0	1	1	1	0	78
short	open	short	short	open	open	open	open	39.47	1	0	0	1	1	1	1	79
short	open	short	open	short	short	short	short	40	1	0	1	0	0	0	0	80
short	open	short	open	short	short	short	open	40.47	1	0	1	0	0	0	1	81
short	open	short	open	short	short	open	short	41	1	0	1	0	0	1	0	82
short	open	short	open	short	short	open	open	41.47	1	0	1	0	0	1	1	83
short	open	short	open	short	open	short	short	42	1	0	1	0	1	0	0	84
short	open	short	open	short	open	short	open	42.47	1	0	1	0	1	0	1	85

short	open	short	open	short	open	open	short	43	1	0	1	0	1	1	0	86
short	open	short	open	short	open	open	open	43.47	1	0	1	0	1	1	1	87
short	open	short	open	open	short	short	short	44	1	0	1	1	0	0	0	88
short	open	short	open	open	short	short	open	44.47	1	0	1	1	0	0	1	89
short	open	short	open	open	short	open	short	45	1	0	1	1	0	1	0	90
short	open	short	open	open	short	open	open	45.47	1	0	1	1	0	1	1	91
short	open	short	open	open	open	short	short	46	1	0	1	1	1	0	0	92
short	open	short	open	open	open	short	open	46.47	1	0	1	1	1	0	1	93
short	open	short	open	open	open	open	short	47	1	0	1	1	1	1	0	94
short	open	short	open	open	open	open	open	47.47	1	0	1	1	1	1	1	95
short	open	open	short	short	short	short	short	48	1	1	0	0	0	0	0	96
short	open	open	short	short	short	short	open	48.47	1	1	0	0	0	0	1	97
short	open	open	short	short	short	open	short	49	1	1	0	0	0	1	0	98
short	open	open	short	short	short	open	open	49.47	1	1	0	0	0	1	1	99
short	open	open	short	short	open	short	short	50	1	1	0	0	1	0	0	100

short	open	open	short	short	open	short	open	50.47	1	1	0	0	1	0	1	101
short	open	open	short	short	open	open	short	51	1	1	0	0	1	1	0	102
short	open	open	short	short	open	open	open	51.47	1	1	0	0	1	1	1	103
short	open	open	short	open	short	short	short	52	1	1	0	1	0	0	0	104
short	open	open	short	open	short	short	open	52.47	1	1	0	1	0	0	1	105
short	open	open	short	open	short	open	short	53	1	1	0	1	0	1	0	106
short	open	open	short	open	short	open	open	53.47	1	1	0	1	0	1	1	107
short	open	open	short	open	open	short	short	54	1	1	0	1	1	0	0	108
short	open	open	short	open	open	short	open	54.47	1	1	0	1	1	0	1	109
short	open	open	short	open	open	open	short	55	1	1	0	1	1	1	0	110
short	open	open	short	open	open	open	open	55.47	1	1	0	1	1	1	1	111
short	open	open	open	short	short	short	short	56	1	1	1	0	0	0	0	112
short	open	open	open	short	short	short	open	56.47	1	1	1	0	0	0	1	113
short	open	open	open	short	short	open	short	57	1	1	1	0	0	1	0	114
short	open	open	open	short	short	open	open	57.47	1	1	1	0	0	1	1	115

short	open	open	open	short	open	short	short	58		1	1	1	0	1	0	0	116
short	open	open	open	short	open	short	open	58.47		1	1	1	0	1	0	1	117
short	open	open	open	short	open	open	short	59		1	1	1	0	1	1	0	118
short	open	open	open	short	open	open	open	59.47		1	1	1	0	1	1	1	119
short	open	open	open	open	short	short	short	60		1	1	1	1	0	0	0	120
short	open	open	open	open	short	short	open	60.47		1	1	1	1	0	0	1	121
short	open	open	open	open	short	open	short	61		1	1	1	1	0	1	0	122
short	open	open	open	open	short	open	open	61.47		1	1	1	1	0	1	1	123
short	open	open	open	open	open	short	short	62		1	1	1	1	1	0	0	124
short	open	open	open	open	open	short	open	62.47		1	1	1	1	1	0	1	125
short	open	open	open	open	open	open	short	63		1	1	1	1	1	1	0	126
short	open	open	open	open	open	open	open	63.47		1	1	1	1	1	1	1	127
open	short	short	short	short	short	short	short	64	1	0	0	0	0	0	0	0	128
open	short	short	short	short	short	short	open	64.47	1	0	0	0	0	0	0	1	129
open	short	short	short	short	short	open	short	65	1	0	0	0	0	0	1	0	130

open	short	short	short	short	short	open	open	65.47	1	0	0	0	0	0	1	1	131
open	short	short	short	short	open	short	short	66	1	0	0	0	0	1	0	0	132
open	short	short	short	short	open	short	open	66.47	1	0	0	0	0	1	0	1	133
open	short	short	short	short	open	open	short	67	1	0	0	0	0	1	1	0	134
open	short	short	short	short	open	open	open	67.47	1	0	0	0	0	1	1	1	135
open	short	short	short	open	short	short	short	68	1	0	0	0	1	0	0	0	136
open	short	short	short	open	short	short	open	68.47	1	0	0	0	1	0	0	1	137
open	short	short	short	open	short	open	short	69	1	0	0	0	1	0	1	0	138
open	short	short	short	open	short	open	open	69.47	1	0	0	0	1	0	1	1	139
open	short	short	short	open	open	short	short	70	1	0	0	0	1	1	0	0	140
open	short	short	short	open	open	short	open	70.47	1	0	0	0	1	1	0	1	141
open	short	short	short	open	open	open	short	71	1	0	0	0	1	1	1	0	142
open	short	short	short	open	open	open	open	71.47	1	0	0	0	1	1	1	1	143
open	short	short	open	short	short	short	short	72	1	0	0	1	0	0	0	0	144
open	short	short	open	short	short	short	open	72.47	1	0	0	1	0	0	0	1	145

open	short	short	open	short	short	open	short	73	1	0	0	1	0	0	1	0	146
open	short	short	open	short	short	open	open	73.47	1	0	0	1	0	0	1	1	147
open	short	short	open	short	open	short	short	74	1	0	0	1	0	1	0	0	148
open	short	short	open	short	open	short	open	74.47	1	0	0	1	0	1	0	1	149
open	short	short	open	short	open	open	short	75	1	0	0	1	0	1	1	0	150
open	short	short	open	short	open	open	open	75.47	1	0	0	1	0	1	1	1	151
open	short	short	open	open	short	short	short	76	1	0	0	1	1	0	0	0	152
open	short	short	open	open	short	short	open	76.47	1	0	0	1	1	0	0	1	153
open	short	short	open	open	short	open	short	77	1	0	0	1	1	0	1	0	154
open	short	short	open	open	short	open	open	77.47	1	0	0	1	1	0	1	1	155
open	short	short	open	open	open	short	short	78	1	0	0	1	1	1	0	0	156
open	short	short	open	open	open	short	open	78.47	1	0	0	1	1	1	0	1	157
open	short	short	open	open	open	open	short	79	1	0	0	1	1	1	1	0	158
open	short	short	open	open	open	open	open	79.47	1	0	0	1	1	1	1	1	159
open	short	open	short	short	short	short	short	80	1	0	1	0	0	0	0	0	160

open	short	open	short	short	short	short	open	80.47	1	0	1	0	0	0	0	1	161
open	short	open	short	short	short	open	short	81	1	0	1	0	0	0	1	0	162
open	short	open	short	short	short	open	open	81.47	1	0	1	0	0	0	1	1	163
open	short	open	short	short	open	short	short	82	1	0	1	0	0	1	0	0	164
open	short	open	short	short	open	short	open	82.47	1	0	1	0	0	1	0	1	165
open	short	open	short	short	open	open	short	83	1	0	1	0	0	1	1	0	166
open	short	open	short	short	open	open	open	83.47	1	0	1	0	0	1	1	1	167
open	short	open	short	open	short	short	short	84	1	0	1	0	1	0	0	0	168
open	short	open	short	open	short	short	open	84.47	1	0	1	0	1	0	0	1	169
open	short	open	short	open	short	open	short	85	1	0	1	0	1	0	1	0	170
open	short	open	short	open	short	open	open	85.47	1	0	1	0	1	0	1	1	171
open	short	open	short	open	open	short	short	86	1	0	1	0	1	1	0	0	172
open	short	open	short	open	open	short	open	86.47	1	0	1	0	1	1	0	1	173
open	short	open	short	open	open	open	short	87	1	0	1	0	1	1	1	0	174
open	short	open	short	open	open	open	open	87.47	1	0	1	0	1	1	1	1	175

open	short	open	open	short	short	short	short	88	1	0	1	1	0	0	0	0	176
open	short	open	open	short	short	short	open	88.47	1	0	1	1	0	0	0	1	177
open	short	open	open	short	short	open	short	89	1	0	1	1	0	0	1	0	178
open	short	open	open	short	short	open	open	89.47	1	0	1	1	0	0	1	1	179
open	short	open	open	short	open	short	short	90	1	0	1	1	0	1	0	0	180
open	short	open	open	short	open	short	open	90.47	1	0	1	1	0	1	0	1	181
open	short	open	open	short	open	open	short	91	1	0	1	1	0	1	1	0	182
open	short	open	open	short	open	open	open	91.47	1	0	1	1	0	1	1	1	183
open	short	open	open	open	short	short	short	92	1	0	1	1	1	0	0	0	184
open	short	open	open	open	short	short	open	92.47	1	0	1	1	1	0	0	1	185
open	short	open	open	open	short	open	short	93	1	0	1	1	1	0	1	0	186
open	short	open	open	open	short	open	open	93.47	1	0	1	1	1	0	1	1	187
open	short	open	open	open	open	short	short	94	1	0	1	1	1	1	0	0	188
open	short	open	open	open	open	short	open	94.47	1	0	1	1	1	1	0	1	189
open	short	open	open	open	open	open	short	95	1	0	1	1	1	1	1	0	190

open	short	open	open	open	open	open	open	95.47	1	0	1	1	1	1	1	1	191
open	open	short	short	short	short	short	short	96	1	1	0	0	0	0	0	0	192
open	open	short	short	short	short	short	open	96.47	1	1	0	0	0	0	0	1	193
open	open	short	short	short	short	open	short	97	1	1	0	0	0	0	1	0	194
open	open	short	short	short	short	open	open	97.47	1	1	0	0	0	0	1	1	195
open	open	short	short	short	open	short	short	98	1	1	0	0	0	1	0	0	196
open	open	short	short	short	open	short	open	98.47	1	1	0	0	0	1	0	1	197
open	open	short	short	short	open	open	short	99	1	1	0	0	0	1	1	0	198
open	open	short	short	short	open	open	open	99.47	1	1	0	0	0	1	1	1	199
open	open	short	short	open	short	short	short	100	1	1	0	0	1	0	0	0	200
open	open	short	short	open	short	short	open	100.47	1	1	0	0	1	0	0	1	201
open	open	short	short	open	short	open	short	101	1	1	0	0	1	0	1	0	202
open	open	short	short	open	short	open	open	101.47	1	1	0	0	1	0	1	1	203
open	open	short	short	open	open	short	short	102	1	1	0	0	1	1	0	0	204
open	open	short	short	open	open	short	open	102.47	1	1	0	0	1	1	0	1	205

open	open	short	short	open	open	open	short	103	1	1	0	0	1	1	1	0	206
open	open	short	short	open	open	open	open	103.47	1	1	0	0	1	1	1	1	207
open	open	short	open	short	short	short	short	104	1	1	0	1	0	0	0	0	208
open	open	short	open	short	short	short	open	104.47	1	1	0	1	0	0	0	1	209
open	open	short	open	short	short	open	short	105	1	1	0	1	0	0	1	0	210
open	open	short	open	short	short	open	open	105.47	1	1	0	1	0	0	1	1	211
open	open	short	open	short	open	short	short	106	1	1	0	1	0	1	0	0	212
open	open	short	open	short	open	short	open	106.47	1	1	0	1	0	1	0	1	213
open	open	short	open	short	open	open	short	107	1	1	0	1	0	1	1	0	214
open	open	short	open	short	open	open	open	107.47	1	1	0	1	0	1	1	1	215
open	open	short	open	open	short	short	short	108	1	1	0	1	1	0	0	0	216
open	open	short	open	open	short	short	open	108.47	1	1	0	1	1	0	0	1	217
open	open	short	open	open	short	open	short	109	1	1	0	1	1	0	1	0	218
open	open	short	open	open	short	open	open	109.47	1	1	0	1	1	0	1	1	219
open	open	short	open	open	open	short	short	110	1	1	0	1	1	1	0	0	220

open	open	short	open	open	open	short	open	110.47	1	1	0	1	1	1	0	1	221
open	open	short	open	open	open	open	short	111	1	1	0	1	1	1	1	0	222
open	open	short	open	open	open	open	open	111.47	1	1	0	1	1	1	1	1	223
open	open	open	short	short	short	short	short	112	1	1	1	0	0	0	0	0	224
open	open	open	short	short	short	short	open	112.47	1	1	1	0	0	0	0	1	225
open	open	open	short	short	short	open	short	113	1	1	1	0	0	0	1	0	226
open	open	open	short	short	short	open	open	113.47	1	1	1	0	0	0	1	1	227
open	open	open	short	short	open	short	short	114	1	1	1	0	0	1	0	0	228
open	open	open	short	short	open	short	open	114.47	1	1	1	0	0	1	0	1	229
open	open	open	short	short	open	open	short	115	1	1	1	0	0	1	1	0	230
open	open	open	short	short	open	open	open	115.47	1	1	1	0	0	1	1	1	231
open	open	open	short	open	short	short	short	116	1	1	1	0	1	0	0	0	232
open	open	open	short	open	short	short	open	116.47	1	1	1	0	1	0	0	1	233
open	open	open	short	open	short	open	short	117	1	1	1	0	1	0	1	0	234
open	open	open	short	open	short	open	open	117.47	1	1	1	0	1	0	1	1	235

open	open	open	short	open	open	short	short	118	1	1	1	0	1	1	0	0	236
open	open	open	short	open	open	short	open	118.47	1	1	1	0	1	1	0	1	237
open	open	open	short	open	open	open	short	119	1	1	1	0	1	1	1	0	238
open	open	open	short	open	open	open	open	119.47	1	1	1	0	1	1	1	1	239
open	open	open	open	short	short	short	short	120	1	1	1	1	0	0	0	0	240
open	open	open	open	short	short	short	open	120.47	1	1	1	1	0	0	0	1	241
open	open	open	open	short	short	open	short	121	1	1	1	1	0	0	1	0	242
open	open	open	open	short	short	open	open	121.47	1	1	1	1	0	0	1	1	243
open	open	open	open	short	open	short	short	122	1	1	1	1	0	1	0	0	244
open	open	open	open	short	open	short	open	122.47	1	1	1	1	0	1	0	1	245
open	open	open	open	short	open	open	short	123	1	1	1	1	0	1	1	0	246
open	open	open	open	short	open	open	open	123.47	1	1	1	1	0	1	1	1	247
open	open	open	open	open	short	short	short	124	1	1	1	1	1	0	0	0	248
open	open	open	open	open	short	short	open	124.47	1	1	1	1	1	0	0	1	249
open	open	open	open	open	short	open	short	125	1	1	1	1	1	0	1	0	250

open	open	open	open	open	short	open	open	125.47	1	1	1	1	1	0	1	1	251
open	open	open	open	open	open	short	short	126	1	1	1	1	1	1	0	0	252
open	open	open	open	open	open	short	open	126.47	1	1	1	1	1	1	0	1	253
open	open	open	open	open	open	open	short	127	1	1	1	1	1	1	1	0	254
open	open	open	open	open	open	open	open	127.47	1	1	1	1	1	1	1	1	255